

The Sedentary Survey of Extreme High Energy Peaked BL Lacs. II. The Catalog and Spectral Properties

P. Giommi¹, S. Piranomonte¹, M. Perri¹, and P. Padovani^{2,3,4}

¹ ASI Science Data Center, ASDC, Agenzia Spaziale Italiana c/o ESRIN, via G. Galilei 00044 Frascati, Italy

² Space Telescope Science Institute, 3700 San Martin Drive, Baltimore, MD 21218, USA

³ Affiliated to the Space Telescope Division of the European Space Agency, ESTEC, Noordwijk, the Netherlands

⁴ ST-ECF, European Southern Observatory, Karl-Schwarzschild-Str. 2, D-85748 Garching bei München, Germany (current address)

Received; accepted

Abstract. The multi-frequency ‘Sedentary Survey’ is a deep, statistically complete, radio flux limited sample comprising 150 BL Lacertae objects distinguished by their extremely high X-ray to radio flux ratio (f_x/f_r), ranging from five hundred to over five thousand times that of typical BL Lacs discovered in radio surveys. This large excess of high energy photons compared to radio emission is thought to be due to synchrotron radiation that in these sources reaches the UV or the X-ray band. The name ‘Sedentary Survey’ originates from the multi-frequency technique used to select the sample that was expected to be so efficient as to allow the conduction of some preliminary statistical studies even without the need to identify the candidates through optical spectroscopy. The details of the selection criteria and the preliminary results have been published in Giommi et al. (1999). In this paper we present the final, 100% identified, catalog together with the optical, X-ray and broad-band Spectral Energy Distributions (SED) constructed combining literature multi-frequency data with non-simultaneous optical observations and *BeppoSAX* X-ray data, when available. The SEDs confirm that the peak of the synchrotron power in these objects is located at very high energies. *BeppoSAX* wide band X-ray observations show that, in most cases, the X-ray spectra are convex and well described by a logarithmic parabola model peaking (in a $\nu f(\nu)$ vs ν representation) between 0.02 to several keV. Although detailed X-ray spectral data are available for only about one fifth of the sources the observed peaks never reach energies well above 10 keV (as in Mkn 501 during the large X-ray flare of April 1997 and in 1ES 2344+514 in December 1996) implying that hard X-ray synchrotron peak energies are rare and probably associated with strong flaring events.

Owing to the high synchrotron energies involved most of the sources in the catalog are likely to be TeV emitters, with the closest and brightest ones probably detectable by the present generation of Cherenkov telescopes. However, only 50% (3 out of 6) of the presently established TeV BL Lacs are actually included in the survey suggesting that the hardest peaks may be associated with secondary synchrotron components that can be detected only above the soft X-ray band. The existence of secondary emission regions is suggested by the strong X-ray spectral curvature that in some objects predicts an optical flux much below the observed emission.

The optical spectrum of about one fourth of the sources is totally featureless hampering any red-shift or luminosity determination. Because this implies that the non-thermal nuclear emission must be well above that of the host galaxy, these objects are likely to be the most powerful sources in the survey and therefore be examples of the yet unreported *high radio luminosity–high energy peaked* BL Lacs. The existence of such objects would be at odds with the claimed inverse proportionality between radio power and synchrotron peak energy known as the “blazar sequence”.

At the low-power end of the luminosity dynamical range, where the non-thermal optical continuum falls below the emission from the host galaxy, recognition issues start becoming important since BL Lacs in this luminosity regime can hardly be recognized as such, but rather as *radio galaxies* or simply as *elliptical galaxies*. We have found a small sample of bright nearby elliptical galaxies that are candidate low radio power high energy peaked BL Lacs.

Key words. galaxies: active - galaxies: BL Lacertae surveys:

1. Introduction

BL Lacertae objects are a rare and very peculiar type of Active Galactic Nuclei (AGN). Their observational properties, which include super-luminal motion, strong and rapidly variable non-

thermal radiation across the entire electromagnetic spectrum and a high degree of polarization, are believed to be the signature of strongly amplified radiation emitted in a relativistic jet closely aligned to the line of sight (e.g. Urry & Padovani (1995)).

These unusual physical and geometrical properties, combined with the peculiar cosmological evolution that distinguishes BL Lacs from other types of AGN, have made this class of sources the subject of intense research activity and of large multi-frequency observation campaigns.

Despite the fact that BL Lacs emit strongly over the entire electromagnetic spectrum, nearly all of presently known sources of this type have been discovered at radio or at X-ray frequencies, or through a combination of these two bands. However, in some still poorly explored observing windows, like the millimeter/microwave region and the gamma-ray/TeV bands, BL Lacs, together with Flat Spectrum Radio Quasars (FSRQ), are expected to be one of the major constituents of the extra-galactic discrete source population. New large samples of these objects will certainly be built when deep surveys based on data from the Planck and GLAST space missions will become available in a few years.

The observed non-thermal emission in BL Lacs is thought to be due to synchrotron emission peaking (in a $\text{Log}(\nu f(\nu)) - \text{Log}(\nu)$ representation) between the far infrared and the hard X-ray band, followed by Inverse Compton scattering up to very high energies. Those BL Lacs where the synchrotron peak is located at low energy (known as Low energy peaked BL Lacs, LBL, Padovani & Giommi (1995)) so far have been discovered mostly in radio surveys, while those where the synchrotron power reaches the UV or the X-ray band (High energy peaked BL Lacs, or HBL) have been discovered much more frequently in X-ray surveys.

The Sedentary Multi-frequency Survey (Giommi et al. (1999), hereafter referred to as Paper I) was designed to assemble a large and statistically well defined sample of HBL BL Lacs by exploiting the fact that the electromagnetic emission of these sources is so extreme that no other type of extra-galactic source type is known to possess a similar Spectral Energy Distribution (SED). By imposing radio, optical and X-ray flux ratios that are only consistent with the unique SEDs of HBL BL Lacs it is then possible to build large samples of these rare objects with very high selection efficiency.

The sample presented in Paper I included 155 BL Lac candidates, only 40% of which were at the time spectroscopically identified. However, it was estimated that the multi-frequency selection technique applied ensured that at least 85% of the candidates were genuine BL Lacs. That allowed the authors to derive, though in a preliminary way, some important statistical properties of HBL BL Lacs, such as their radio LogN-LogS and Cosmological evolution. For that reason the survey was named ‘‘Sedentary’’.

The estimation of some of the fundamental properties of the sample, however, require the knowledge of luminosity, hence redshift which makes an identification campaign clearly necessary. This need prompted the organization of a dedicated optical spectroscopy observation program (see Piranomonte et al. (2004), hereafter Paper III) that, together with data collected by other independent groups, mostly aimed at the systematic identification of bright high Galactic latitude RASS sources (Schwope et al. (2000), Bauer et al. (2000), Beckmann (2000), Anderson et al. (2003)), led to the identification of *all* the candidates in the sample.

In this paper we present the complete cleaned sample, which now includes 150 objects following i) the removal of those candidates that the spectroscopic identification campaign did not confirm to be BL Lacs, and ii) the addition of 7 new BL Lacs that satisfy all criteria for inclusion in the survey but were not in the original sample because their α_{ro} was just below the threshold of 0.2 due to the optical contamination from the host galaxy which was not taken into account.

We also present a detailed spectral analysis based on broad band *BeppoSAX* archival data and the radio to X-ray SED of a selection of objects built using multi-frequency literature data, on our own optical observations and *BeppoSAX* data, when available.

The radio LogN-LogS, luminosity function and cosmological evolution have been presented in preliminary form in Paper I and in Perri et al. (2002), the final results are presented in a dedicated paper (Giommi et al. (2004), hereafter Paper IV).

2. The sample

A complete description of the Sedentary Survey sample is given in Paper I, in this section we summarize the main selection criteria and we refer the reader to the original paper for more details.

The sample was extracted from a large set of radio and X-ray emitting sources selected through a cross-correlation between the RASS catalog of bright X-ray sources (Voges et al. (1999)) and the NVSS catalog of radio (1.4 GHz, Condon et al. (1998)) sources. The following conditions were imposed to avoid the complications due to the Galactic plane and ensure that the sample is statistically complete above the radio flux limit of $f_{\text{r}} = 3.5$ mJy

1. $|b| > 20^\circ$;
2. $f_{\text{x}}/f_{\text{r}} \geq 3 \times 10^{-10} \text{ erg cm}^{-2} \text{ s}^{-1} \text{ Jy}^{-1}$;
3. $\alpha_{\text{ro}} > 0.2$;
4. $f_{\text{r}} \geq 3.5$ mJy;
5. RASSBSC count rate ≥ 0.1 cts/s;
6. $V \leq 21$;

where α_{ro} is the usual broad band spectral index between the radio (5GHz) and optical (5000 Å) fluxes and V is the visual apparent magnitude of the optical counterpart.

Condition 1) limits the survey area to high Galactic latitude regions where soft X-ray absorption due to Galactic N_{H} is low; condition 2) imposes a very large $f_{\text{x}}/f_{\text{r}}$ flux ratio that can be reached by HBL BL Lacs only; condition 3) removes from the sample radio quiet sources, such as nearby Seyfert galaxies where the unrelated radio and X-ray flux may accidentally satisfy condition 2); condition 4), 5) and 6) are necessary to ensure statistical completeness above $f_{\text{r}} \geq 3.5$ mJy.

3. The Catalog

The fully identified complete sample including 150 extreme HBL BL Lacs is presented in Table 1 where column 1 gives the source name built with the catalog identification code SHBL (where S stands for ‘‘Sedentary’’ survey and HBL for High

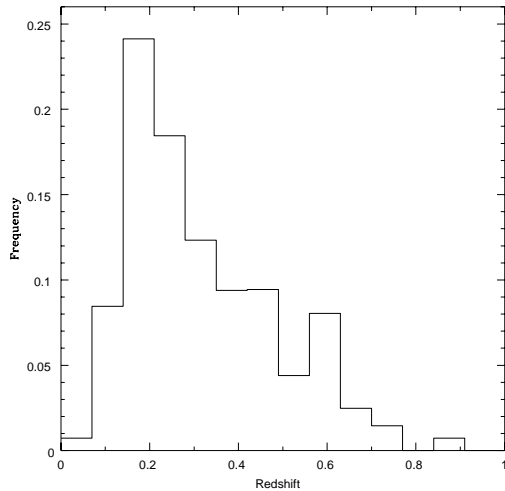


Fig. 1. The redshift distribution of the subsample of 111 BL Lacs with a measured redshift after de-convolving for the X-ray sky coverage of the survey (see also Landt et al. (2001)).

energy peaked BL Lacs, Padovani & Giommi (1995)) and the arc-second precision optical coordinates of the source taken from the APM (Irwin et al. (1994)) and COSMOS (Yentis et al. (1992)) on-line services; column 2 gives the RASS name; column 3, 4 and 5 give the X-ray flux (0.1-2.4 keV), the radio flux (20 cm, from the NVSS survey), and the optical apparent V magnitude (from APM and COSMOS, see Paper I) respectively; column 6 gives the redshift, when available; column 7 gives the reference for the optical identification.

The catalog is also available on the web at the following address

<http://www.asdc.asi.it/sedentary/>

where additional data, including the broad band spectral energy distributions, finding charts and optical spectra (from Paper III) are also provided, when available.

Redshifts were measured for 111 BL Lacs, mostly from spectral features due to the host galaxy. The other 39 sources ($\sim 25\%$ of the sample) remain without redshift since their optical spectrum does not show any emission or absorption lines.

The sample is flux limited, complete (that is *all* the sources above the flux limit are included) and 100% identified and is therefore suitable for an unbiased investigation of the statistical properties of the population that it represents.

The main cosmological properties, such as radio LogN-LogS, luminosity function and cosmological evolution, are studied in detail in Paper IV; in the following we provide only some basic statistics of the parameters listed in Table 1. The redshift and V distributions, corrected for the X-ray sky coverage of the survey, are shown in Figs. 1 and 2 respectively. The average redshift of the subsample of 111 objects for which a value could be measured is $\langle z \rangle = 0.32$ and is rather low compared to other radio loud AGN of similar or even higher radio flux (e.g. Padovani et al. (2003)), but consistent with earlier results about X-ray selected BL Lacs that have demonstrated the peculiar cosmological evolution of these sources (Bade et al.

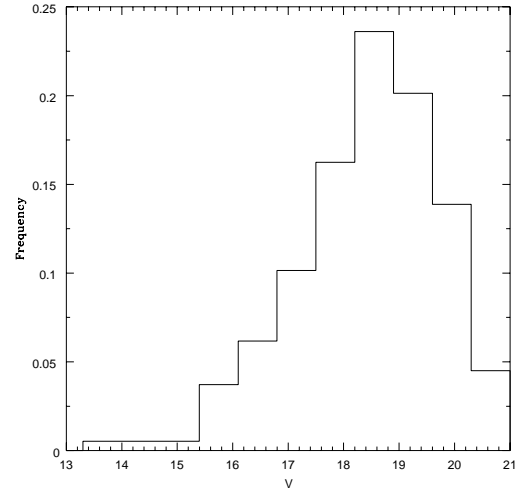


Fig. 2. The sky coverage corrected distribution of optical apparent magnitudes (V) of all sources in the Sedentary survey. Note that the fraction of sources with $V \geq 20$ is very low suggesting that the condition 6 in the definition of the sample ($V \leq 21$) only excluded a tiny fraction of sources.

(1998a), Rector et al. (2000)). However, the exclusion of the 39 sources without a redshift determination, which may well be distant, high luminosity objects (see below) implies that this value is likely to be only a lower limit.

The distribution of optical magnitudes (see Fig. 2) is sharply peaked around the mean value of $\langle V \rangle = 18.4$ and only a few sources are fainter than $V \approx 20$. Condition number 6 in the sample definition criteria (i.e. $V \leq 21$) should therefore exclude a very small fraction of BL Lacs ($\lesssim 1 - 2\%$, see also Paper I).

3.1. Notes on individual objects

3.1.1. SHBL J040128.0+815312

This source has been identified as an early-type galaxy by Bauer et al. (2000) but its X-ray and radio luminosities are rather high (about 5×10^{44} erg/s and 3×10^{31} erg/s/Hz respectively). It is therefore likely that this source is a AGN, in the following we will assume that it is a BL Lac.

3.1.2. SHBL J114535.1-034001, SHBL J235023.2-243603

These X-ray/radio sources are within clusters of galaxies. However, since i) the RASS X-ray emission in these sources is not extended, ii) the radio emission coincides with a galaxy, and iii) from our optical spectroscopic campaign we have found that the Ca H&K break in their optical spectrum is diluted by non-thermal radiation. We assume that these objects are BL Lacs in clusters.

Table 1. The complete sample of HBL BL Lacs in the Sedentary Survey: objects coordinates and main properties

Source name	RASS name (1RXS J)	$f_{0.1-2.4 \text{ keV}}$ [erg/cm ² /s]	$f_{20 \text{ cm}}$ [mJy]	V	z	Ref. for opt. ID
(1)	(2)	(3)	(4)	(5)	(6)	(7)
SHBL J001355.9–185406	001356.6–18540	1.26×10^{-11}	29.6	16.8	0.095	(a)
SHBL J001527.9+353639	001528.3+35364	3.45×10^{-12}	11.2	18.3	...	(*)
SHBL J001827.8+294729	001827.8+29473	1.43×10^{-11}	33.8	18.5	0.100	(b)
SHBL J003334.2–192133	003334.6–19213	1.49×10^{-11}	18.9	16.1	0.610	(a), (*)
SHBL J003514.7+151504	003514.9+15151	7.33×10^{-12}	18.8	17.1	0.250	(a)
SHBL J004208.0+364112	004208.1+36411	3.68×10^{-12}	12.0	18.0	...	(a), (*)
SHBL J005816.8+172310	005817.1+17230	8.38×10^{-12}	9.4	19.2	...	(a)
SHBL J011050.0–125502	011050.0–12545	1.51×10^{-11}	17.5	17.4	0.234	(b)
SHBL J011501.9–340028	011501.3–34000	2.20×10^{-12}	6.4	20.1	0.482	(*)
SHBL J011747.0–244333	011746.6–24432	3.82×10^{-12}	10.3	19.0	0.279	(*)
SHBL J012308.7+342049	012308.9+34204	6.14×10^{-11}	45.7	15.2	0.272	(c)
SHBL J012338.2–231058	012338.2–23110	9.03×10^{-12}	27.6	18.7	0.404	(a)
SHBL J012657.2+330730	012657.1+33073	4.75×10^{-12}	7.1	17.5	...	(*)
SHBL J013632.5+390559	013632.9+39055	2.33×10^{-11}	60.6	15.4	...	(a), (*)
SHBL J014040.7–075848	014040.9–07585	1.19×10^{-11}	27.4	18.3	...	(d)
SHBL J020106.3+003401	020106.3+00340	6.85×10^{-12}	13.4	18.0	0.299	(e)
SHBL J020412.8–333342	020413.6–33334	2.54×10^{-12}	6.4	18.6	0.617	(*)
SHBL J020838.1+352313	020837.5+35231	6.99×10^{-12}	5.0	19.2	0.318	(f)
SHBL J021630.9+231513	021632.3+23144	1.40×10^{-11}	35.9	19.2	0.288	(g)
SHBL J022716.6+020158	022716.6+02015	3.93×10^{-11}	37.0	18.2	...	(a)
SHBL J023536.6–293843	023536.7–29384	2.81×10^{-12}	5.5	17.6	...	(a)
SHBL J025018.8–212940	025018.2–21295	4.78×10^{-12}	3.8	19.8	0.498	(a)
SHBL J030330.2+055430	030330.0+05542	1.16×10^{-11}	29.7	17.4	0.196	(b)
SHBL J030416.3–283217	030416.4–28321	4.95×10^{-12}	8.3	19.3	...	(d)
SHBL J031422.9+061956	031422.7+06200	2.29×10^{-11}	29.4	18.0	...	(a)
SHBL J031633.7–221611	031634.6–22161	2.44×10^{-12}	4.4	19.0	0.228	(*)
SHBL J031951.9+184534	031951.9+18453	2.70×10^{-11}	22.9	18.1	0.190	(f)
SHBL J032350.7+071736	032350.5+07174	6.69×10^{-12}	4.5	20.3	...	(*)
SHBL J032541.0–164618	032540.8–16460	5.87×10^{-11}	27.6	16.0	0.291	(a)
SHBL J032613.9+022515	032613.6+02252	3.36×10^{-11}	68.3	17.4	0.147	(h)
SHBL J034923.2–115927	034922.8–11592	3.09×10^{-11}	24.9	18.2	0.185	(i)
SHBL J035856.1–305448	035855.6–30543	4.86×10^{-12}	13.2	18.5	...	(d)
SHBL J040128.0+815312	040129.1+81532	3.55×10^{-12}	9.7	17.6	0.215	(a)
SHBL J040324.5–242950	040324.1–24293	5.01×10^{-12}	7.4	20.2	0.357	(*)
SHBL J041112.2–394143	041112.1–39413	4.10×10^{-12}	5.3	18.8	...	(*)
SHBL J041652.4+010524	041652.6+01053	7.32×10^{-11}	120.7	17.5	0.287	(h)
SHBL J042132.8–062905	042132.7–06284	6.45×10^{-12}	16.0	20.1	0.390	(a)
SHBL J042218.4+195051	042218.2+19504	9.98×10^{-12}	9.0	20.3	0.516	(f)
SHBL J042900.1–323640	042900.5–32363	5.81×10^{-12}	9.3	17.6	...	(d)
SHBL J044018.5–245933	044017.8–24591	4.06×10^{-12}	12.7	19.5	...	(d)
SHBL J044127.4+150456	044127.8+15045	3.93×10^{-11}	14.0	19.8	0.109	(*)
SHBL J044230.1–001830	044229.8–00182	4.06×10^{-12}	4.2	20.0	0.449	(*)
SHBL J050335.3–111507	050335.6–11150	1.29×10^{-11}	10.5	17.9	...	(*)
SHBL J050939.0–040036	050938.3–04003	2.70×10^{-11}	71.2	19.0	0.304	(h)
SHBL J050939.8–251403	050940.0–25135	2.13×10^{-12}	4.5	20.1	0.264	(*)
SHBL J060714.3–251859	060714.2–25185	4.13×10^{-12}	12.2	18.9	0.275	(*)
SHBL J062149.6–341149	062150.0–34114	4.47×10^{-12}	8.8	18.7	0.529	(*)
SHBL J071219.0+571948	071218.9+57193	3.13×10^{-12}	8.0	19.9	0.095	(l)
SHBL J074405.6+743358	074405.6+74335	1.36×10^{-11}	23.4	16.9	0.315	(f)
SHBL J075124.9+173051	075124.3+17304	3.85×10^{-12}	10.5	17.4	0.185	(a), (*)
SHBL J075324.6+292132	075322.4+29215	2.78×10^{-12}	4.3	18.7	0.161	(*)
SHBL J083251.3+330009	083251.9+33001	3.33×10^{-12}	4.5	20.8	0.671	(m)
SHBL J084712.9+113350	084713.3+11334	2.38×10^{-11}	33.3	17.2	0.199	(n)
SHBL J085909.9+834459	085916.5+83445	3.63×10^{-12}	10.3	17.5	0.327	(o)
SHBL J091322.2+813304	091324.6+81331	3.56×10^{-12}	5.1	19.8	0.639	(o)

Table 1. The complete sample of HBL BL Lacs in the Sedentary Survey: objects coordinates and main properties - Continued

Source name	RASS name (1RXS J)	$f_{0.1-2.4 \text{ keV}}$ [erg/cm ² /s]	$f_{20 \text{ cm}}$ [mJy]	V	z	Ref. for opt. ID
(1)	(2)	(3)	(4)	(5)	(6)	(7)
SHBL J092401.1+053345	092401.1+05335	5.15×10^{-12}	7.6	18.4	...	(a), (*)
SHBL J093037.5+495025	093037.1+49502	2.69×10^{-11}	21.6	17.2	0.188	(c)
SHBL J094355.5-070951	094355.3-07094	2.88×10^{-12}	7.3	19.9	0.433	(*)
SHBL J095224.0+750213	095225.8+75021	4.83×10^{-12}	12.4	17.2	0.179	(a), (*)
SHBL J095805.9-031740	095806.4-03172	2.82×10^{-12}	7.6	19.6	...	(*)
SHBL J100656.4+345445	100656.9+34544	2.05×10^{-12}	6.7	19.0	0.612	(o)
SHBL J100811.4+470519	100811.5+47052	1.13×10^{-11}	4.9	18.4	0.343	(m)
SHBL J101015.9-311908	101015.9-31190	2.83×10^{-11}	74.4	17.3	0.143	(*)
SHBL J101616.7+410812	101616.4+41081	7.59×10^{-12}	15.0	18.9	0.270	(p)
SHBL J102212.6+512358	102212.5+51240	5.16×10^{-12}	5.3	18.1	0.141	(f)
SHBL J102243.8-011302	102244.2-01125	1.31×10^{-11}	36.3	15.5	...	(a), (*)
SHBL J103118.6+505335	103118.6+50534	5.58×10^{-11}	38.1	16.6	0.361	(q)
SHBL J104651.4-253545	104651.9-25354	4.53×10^{-12}	14.3	19.2	0.254	(*)
SHBL J105125.3+394325	105125.1+39432	4.48×10^{-12}	11.0	18.4	0.498	(o)
SHBL J105606.6+025213	105607.0+02521	1.49×10^{-11}	4.5	17.7	0.236	(a)
SHBL J105723.1+230317	105723.5+23031	6.41×10^{-12}	8.1	18.7	0.379	(r)
SHBL J110021.1+401927	110021.3+40193	7.60×10^{-12}	18.4	17.8	0.225	(o)
SHBL J110337.6-232931	110337.7-23293	5.09×10^{-11}	121.1	16.1	0.186	(h)
SHBL J110427.3+381231	110427.1+38123	2.71×10^{-10}	768.6	14.4	0.031	(s)
SHBL J111130.9+345203	111131.2+34521	7.05×10^{-12}	8.6	19.2	0.212	(m)
SHBL J111706.3+201407	111706.3+20141	5.42×10^{-11}	103.2	15.7	0.139	(g)
SHBL J111939.5-304720	111941.0-30465	3.72×10^{-12}	9.6	19.5	0.412	(*)
SHBL J112048.0+421212	112047.5+42121	1.37×10^{-11}	24.2	17.3	0.124	(c)
SHBL J112348.9+722958	112349.2+72300	6.98×10^{-12}	12.6	18.5	...	(g)
SHBL J113444.5-172902	113443.6-17285	3.64×10^{-12}	5.1	19.7	0.571	(*)
SHBL J113630.3+673704	113630.9+67370	2.38×10^{-11}	45.9	16.7	0.135	(t)
SHBL J113755.4-171042	113755.4-17103	4.72×10^{-12}	5.3	18.9	0.600	(*)
SHBL J114535.1-034001	114535.8-03394	7.96×10^{-12}	19.8	18.4	0.167	(d), (*)
SHBL J114755.0+220539	114754.9+22054	3.77×10^{-12}	4.3	18.3	0.276	(o)
SHBL J114930.3+243926	114930.4+24392	9.73×10^{-12}	28.6	18.0	0.402	(o)
SHBL J115404.4-001010	115404.9-00100	4.81×10^{-12}	10.7	18.7	0.253	(e)
SHBL J121158.6+224232	121158.1+22423	8.25×10^{-12}	20.3	18.5	0.455	(o)
SHBL J122121.9+301037	122121.7+30104	3.16×10^{-11}	71.6	16.4	0.182	(a)
SHBL J123417.1-385635	123416.9-38563	6.10×10^{-12}	7.0	18.0	0.236	(*)
SHBL J123511.0-140322	123511.1-14033	2.63×10^{-12}	4.2	19.8	0.407	(*)
SHBL J123705.5+302004	123705.6+30200	1.06×10^{-11}	5.8	20.5	0.700	(m)
SHBL J123739.0+625842	123739.2+62584	4.03×10^{-12}	12.6	18.6	0.297	(f)
SHBL J124149.3-145558	124149.8-14555	1.81×10^{-11}	17.3	17.3	...	(c), (*)
SHBL J125015.5+315559	125015.0+31560	1.88×10^{-12}	5.7	19.5	...	(*)
SHBL J125134.9-295843	125135.2-29582	4.37×10^{-12}	10.5	19.0	0.487	(c)
SHBL J125300.9+382626	125301.0+38262	6.45×10^{-12}	4.9	19.2	0.372	(a)
SHBL J125341.1-393159	125341.2-39320	1.96×10^{-11}	50.1	18.3	0.179	(*)
SHBL J125731.9+241240	125731.7+24124	1.17×10^{-11}	14.9	15.4	0.141	(c)
SHBL J125847.8-044745	125847.7-04474	7.93×10^{-12}	4.3	18.9	0.586	(a)
SHBL J131155.7+085342	131156.0+08534	4.74×10^{-12}	5.5	19.6	0.469	(a)
SHBL J133529.7-295037	133530.6-29503	7.24×10^{-12}	10.8	19.1	0.513	(f)
SHBL J140630.1-393509	140630.3-39350	4.04×10^{-12}	8.8	19.8	...	(*)
SHBL J140630.2+123620	140630.1+12363	2.56×10^{-12}	6.3	20.6	...	(*)
SHBL J140659.2+164207	140659.1+16420	5.43×10^{-12}	8.4	18.0	...	(a), (*)
SHBL J140918.9+135239	140918.9+13523	2.87×10^{-12}	7.3	20.4	0.580	(a)
SHBL J141756.1+254356	141756.8+25432	2.70×10^{-11}	89.7	16.0	0.237	(h)
SHBL J142239.0+580155	142239.1+58015	2.50×10^{-11}	13.4	18.4	0.638	(m)
SHBL J142739.5-252102	142740.6-25210	4.70×10^{-12}	3.7	18.9	0.318	(*)
SHBL J142832.6+424024	142832.6+42402	5.25×10^{-11}	58.9	16.4	0.130	(h)
SHBL J143917.4+393243	143917.7+39324	1.79×10^{-11}	42.9	16.6	0.344	(a), (*)

Table 1. The complete sample of HBL BL Lacs in the Sedentary Survey: objects coordinates and main properties - Continued

Source name	RASS name (1RXS J)	$f_{0.1-2.4 \text{ keV}}$ [erg/cm ² /s]	$f_{20 \text{ cm}}$ [mJy]	V	z	Ref. for opt. ID
(1)	(2)	(3)	(4)	(5)	(6)	(7)
SHBL J144506.3-032612	144505.9-03261	7.80×10^{-12}	21.8	17.4	...	(a), (*)
SHBL J150340.6-154113	150343.0-15410	2.39×10^{-11}	5.9	17.5	...	(a), (*)
SHBL J150637.0-054004	150636.4-05401	5.03×10^{-12}	15.3	19.5	0.518	(*)
SHBL J151041.0+333504	151040.8+33351	4.45×10^{-12}	9.1	17.0	0.112	(d), (*)
SHBL J151618.6-152343	151618.7-15234	1.46×10^{-11}	8.6	18.7	...	(a), (*)
SHBL J151747.4+652523	151747.3+65252	2.30×10^{-11}	37.8	15.9	0.702	(u)
SHBL J153311.3+185428	153311.7+18542	1.42×10^{-11}	23.0	17.7	0.305	(a), (*)
SHBL J153500.9+532037	153501.1+53204	1.79×10^{-11}	18.4	17.6	0.890	(m)
SHBL J160518.9+542059	160518.5+54210	6.26×10^{-12}	7.8	19.0	0.21	(e)
SHBL J161204.6-043815	161204.4-04381	4.40×10^{-12}	4.3	18.9	...	(*)
SHBL J161632.9+375602	161633.4+37555	1.47×10^{-12}	4.6	18.7	0.204	(*)
SHBL J163123.5+421703	163124.7+42165	6.59×10^{-12}	7.5	19.2	0.468	(m)
SHBL J163658.4-124837	163658.7-12483	8.74×10^{-12}	26.3	20.1	0.246	(*)
SHBL J174702.3+493801	174702.0+49380	2.81×10^{-12}	7.9	19.9	0.460	(*)
SHBL J175615.9+552217	175615.5+55221	1.48×10^{-11}	16.9	17.6	...	(a), (*)
SHBL J175713.4+703336	175712.8+70333	8.68×10^{-12}	10.9	18.3	0.407	(f)
SHBL J184822.3+653657	184822.6+65370	4.29×10^{-12}	9.7	18.3	0.364	(*)
SHBL J203844.8-263633	203845.1-26362	4.73×10^{-12}	5.7	18.5	0.437	(*)
SHBL J204735.8-290859	204737.0-29090	3.97×10^{-12}	10.7	19.3	0.333	(*)
SHBL J204921.7+003926	204921.6-00393	4.85×10^{-12}	6.0	18.1	0.256	(*)
SHBL J205242.7+081038	205242.6+08103	4.90×10^{-12}	6.2	19.6	...	(*)
SHBL J213135.4-091523	213135.5-09152	1.58×10^{-11}	43.6	16.7	0.449	(a), (*)
SHBL J213151.3-251558	213151.7-25160	6.04×10^{-12}	11.0	17.3	...	(*)
SHBL J213852.5-205348	213852.9-20535	1.33×10^{-11}	11.5	17.9	0.290	(a), (*)
SHBL J215852.0-301331	215852.2-30133	5.72×10^{-10}	490.3	13.5	0.117	(v)
SHBL J220155.8-170702	220156.0-17065	5.12×10^{-12}	4.8	18.1	0.169	(a)
SHBL J222253.8-175321	222253.9-17531	2.88×10^{-12}	5.7	19.4	0.297	(*)
SHBL J223812.7-394020	223812.7-39401	6.21×10^{-12}	20.4	18.6	0.250	(d)
SHBL J224340.1-123100	224341.9-12310	9.45×10^{-12}	10.7	18.1	0.226	(b)
SHBL J224910.7-130002	224911.1-13000	9.73×10^{-12}	7.6	18.9	...	(a), (*)
SHBL J225147.3-320614	225146.9-32061	3.61×10^{-12}	3.6	19.0	...	(a), (*)
SHBL J230436.8+370507	230437.1+37050	1.85×10^{-11}	23.1	17.8	...	(a), (*)
SHBL J230634.9-110348	230636.0-11035	5.19×10^{-12}	11.5	19.2	...	(a)
SHBL J230722.0-120518	230722.5-12052	2.94×10^{-12}	7.3	18.6	...	(*)
SHBL J230846.7-221949	230846.7-22195	8.29×10^{-12}	6.5	16.0	0.137	(f)
SHBL J231028.0-371909	231027.0-37192	1.97×10^{-12}	6.3	17.8	...	(*)
SHBL J234333.8+344004	234332.5+34395	1.51×10^{-11}	35.0	20.1	0.366	(*)
SHBL J235023.2-243603	235023.6-24355	2.14×10^{-12}	6.8	18.3	0.193	(a), (*)
SHBL J235730.0-171805	235730.1-17180	2.14×10^{-11}	44.5	17.3	...	(d)
SHBL J235907.9-303739	235908.0-30374	6.50×10^{-11}	65.0	17.0	0.165	(a)

(*) Piranomonte et al. (2004); (a) Bauer et al. (2000); (b) Fisher et al. (1998); (c) Padovani & Giommi (1995); (d) Schwöpe et al. (2000); (e) Sloan Digital Sky Survey (2001); (f) Rector et al. (2000); (g) Bohringer et al. (2000); (h) NED Redshift (1992); (i) Schachter et al. (1993); (l) Beckmann (2000); (m) Bade et al. (1998a); (n) Landt et al. (2001); (o) Beckmann et al. (2003); (p) Cao et al. (1999); (q) Polonsky et al. (1997); (r) White et al. (2000); (s) De Vaucouleurs et al. (1991); (t) Bade et al. (1994); (u) Beckmann et al. (1999); (v) Falomo et al. (1993).

Table 2. List of candidate low luminosity HBLs

Source name	RASS name (1RXS J)	Other name	Redshift	V	X-ray luminosity (erg/s)	Classification
(1)	(2)	(3)	(4)	(5)	(6)	(7)
SHBL J020014.8+312545	020014.5+31254	NGC0777	0.017	12.8	5.6×10^{42}	Elliptical
SHBL J025251.8-011629	025250.3-01160	NGC1132	0.023	7.6	1.1×10^{43}	Elliptical
SHBL J033851.7-353536	033851.5-35354	NGC1404	0.006	10.5	5.9×10^{41}	Elliptical
SHBL J044255.9-263509	044255.9-26345	1WGA J0442.9-2635	N.A.	15.5	...	S0
SHBL J150111.2+014208	150111.6+01415	NGC5813	0.006	11.7	2.2×10^{42}	Elliptical

Table 3. List of the 19 emission line AGNs in the HBL zone

RASS name	$f_{0.1-2.4 \text{ keV}}$ [erg/cm ² /s]	$f_{20 \text{ cm}}$ [mJy]	V	z	Luminosity _{20 cm} [erg/s/Hz]	α_{ro}	Ref. for opt. ID
(1)	(2)	(3)	(4)	(5)	(6)	(7)	(8)
1RXS J000729.3+02405	3.08×10^{-12}	7.6	18.0	0.300	1.68×10^{31}	0.26	(a)
1RXS J013526.9-04263	9.04×10^{-12}	8.2	17.5	0.155	4.32×10^{30}	0.24	(b)
1RXS J023727.6-26302	2.52×10^{-12}	5.6	20.2	0.141	2.41×10^{30}	0.24	(*)
1RXS J023832.1+02333	4.10×10^{-12}	10.4	17.1	0.209	1.04×10^{31}	0.22	(c)
1RXS J035018.4-22170	7.00×10^{-12}	19.1	16.6	0.111	4.98×10^{30}	0.24	(d)
1RXS J035245.6-23425	4.30×10^{-12}	4.3	18.1	0.140	1.83×10^{30}	0.23	(e)
1RXS J035432.5-13400	4.90×10^{-12}	15.8	17.0	0.077	1.92×10^{30}	0.25	(b)
1RXS J084206.6+07593	8.33×10^{-12}	17.4	17.8	0.134	6.73×10^{31}	0.32	(f)
1RXS J092554.3+40041	4.56×10^{-12}	13.2	17.4	0.470	8.09×10^{31}	0.26	(g)
1RXS J093318.2-17144	6.25×10^{-12}	20.2	16.7	0.313	4.91×10^{31}	0.24	(b)
1RXS J122044.5+69053	5.38×10^{-12}	8.2	17.1	0.110	2.10×10^{30}	0.21	(h)
1RXS J123802.1+36164	1.89×10^{-12}	4.9	19.4	0.383	1.84×10^{31}	0.33	(*)
1RXS J130350.5-39503	4.96×10^{-12}	13.6	17.4	0.121	4.17×10^{30}	0.27	(*)
1RXS J133950.5+15593	2.01×10^{-12}	4.6	18.0	0.277	8.45×10^{30}	0.22	(*)
1RXS J170817.7-03493	5.10×10^{-12}	4.8	17.5	0.180	3.48×10^{30}	0.19	(*)
1RXS J172202.0+43152	6.27×10^{-12}	9.0	18.4	0.139	3.76×10^{30}	0.31	(b)
1RXS J182042.7+38171	6.59×10^{-12}	7.5	18.8	0.077	9.88×10^{29}	0.33	(*)
1RXS J212516.7-25553	2.72×10^{-12}	5.2	18.2	0.343	1.54×10^{31}	0.25	(*)
1RXS J222944.5-27553	2.39×10^{-12}	7.8	18.8	0.322	2.02×10^{31}	0.33	(*)

(*) our data; (a) Hewett et al. (1995); (b) Bauer et al. (2000); (c) Schneider et al. (1994); (d) Reimers et al. (1996); (e) Voges et al. (1999); (f) Bade et al. (1998b); (g) Buchalter et al. (1998); (h) Puchnarewicz et al. (1992);

4. Optical Spectroscopy

In Paper I only about 40% of the sources in the sample were confirmed BL Lacs. Although several other candidates were subsequently identified in a number of projects dedicated to the optical follow up observations of bright Rosat X-ray sources (Schwope et al. (2000), Bauer et al. (2000), Beckmann (2000)), many objects would have remained unidentified without a dedicated optical spectroscopy program. We have therefore carried out an extensive optical identification campaign using the Kitt Peak National Observatory 4m telescope, the ESO 3.6m telescope at La Silla and the TNG 3.6m telescope at La Palma, which allowed us to identify *all* sources of the survey. The results are described in detail in Paper III; in the following we summarize the main results.

Good quality optical spectra were obtained for the 76 objects which were either previously unidentified (58) or had been reported in the literature as BL Lacs (18) but no redshift was given and no information about the quality of the optical spectrum was reported (see Table 1). Out of the 58 unclassified candidates 50 were confirmed to be BL Lacs and 8 sources turned out to be emission line AGN.

The full set of spectra are reported and discussed in Paper III. In this paper we show the optical spectra of four representative sources located at different redshifts, (see Fig. 3) plotted in $\text{Log}(\nu f(\nu))$ vs $\text{Log}(\nu)$ space which is normally used to plot broad band Spectral Energy Distributions (SED). We have chosen this graphical representation because it is particularly effective in enhancing broad features and changes in the spectral shape.

The data have been de-reddened and converted to units suitable for $\nu f(\nu)$ vs ν SED plots with the IRAF¹ packages *noao.onedspec.deredden* and *noao.onedspec.splot*.

Figure 3 illustrates how the emitted power at optical frequencies is a blend between the optical output from the host galaxy (steep component), which dominates the spectrum at frequencies below the Ca H&K break, and the non-thermal nuclear emission (flat component), that usually appears at frequencies above the Ca H&K break. The clear trend in the balance between the non-thermal and the galaxian component with redshift strongly indicates that high redshift (which on average implies high luminosity in a flux limited sample) sources are characterized by a flat, featureless optical spectrum. In sources located at redshifts higher than 0.7-0.8 the Ca H&K break falls outside the optical band and the non-thermal emission, which at these distances and radio flux above the survey limit is much brighter than the typical host galaxy, completely dominates the optical spectrum. This calls for a high redshift location of the 39 sources in the sample whose optical spectrum is flat and completely featureless (see discussion in Sect. 4.2). An estimate of a lower limit to the redshift of these sources will be given in Paper III and Paper IV.

4.1. Elliptical galaxies or low luminosity BL Lacs?

Since the luminosity of BL Lac host galaxies (giant ellipticals) is approximately constant (Wurtz et al. (1997), Urry et al. (2000)) the blend between the non-thermal nuclear emission and the optical flux from the host galaxy must be a strong function of the luminosity of the BL Lac. This implies that at the low and high luminosity ends of the radio luminosity function the appearance of the optical spectrum of BL Lacs must be very different, as discussed in the previous paragraph and shown in Fig. 3 (see also Landt et al. (2002)). In particular, the optical emission of low redshift-low luminosity BL Lacs, must be almost completely dominated by the emission from the host galaxy. An example of this effect is shown in Fig. 4 where the non-thermal component of SHBL J044127.4+150456, a $z=0.109$ BL Lac, is barely detectable only at frequencies above the Ca H&K break. At even lower redshifts ($z \lesssim 0.1$) the host galaxy totally dominates the spectrum and distinguishing between normal radio galaxies and BL Lacs becomes very difficult.

In this luminosity regime the X-ray to radio flux ratio (f_x/f_r) remains unaffected, but α_{ro} is heavily contaminated by starlight and could decrease significantly pushing these low luminosity BL Lacs over the borderline between the HBL zone and the radio quiet zone ($\alpha_{ro} < 0.2$) thus biasing the sample at low luminosities. One object of this type, the elliptical galaxy IC1459, was recently associated with a BL Lac by Giommi et al. (2002c).

We have been looking for similar bright elliptical galaxies/low luminosity HBLs in the original sample of high f_x/f_r sources of Paper I ($f_x/f_r \geq 3 \times 10^{-10} \text{ erg cm}^{-2} \text{ s}^{-1} \text{ Jy}^{-1}$) among the objects that were excluded because their α_{ro} was below the threshold value of 0.2. We have found the five objects that are reported in Table 2 where columns 1,2 and 3 give the SHBL, the RASS and other names; column 4 gives the redshift, when available; column 5 is the visual apparent magnitude; column 6 is the X-ray luminosity in the Rosat band and column 7 gives the source classification from NED. As an example Fig. 5 shows the optical image, taken from the ESO on-line service, of one of the objects in Table 2 (1RXS J020014.5+31254=NGC 0777) with the radio iso-intensity contours and the precise position from the NVSS survey overlaid. The flat/inverted radio spectrum ($\alpha_{1.4-2.38\text{GHz}} = -0.37 \pm 0.4$, $F(\nu) \propto \nu^{-\alpha}$) coincident with the nucleus of the galaxy and the f_x/f_r flux ratio make this source consistent with a high energy peaked BL Lac.

4.2. High luminosity HBLs and the problem of redshift estimation

At the bright end of the BL Lac radio luminosity function, especially for the case of HBL objects where, for the same radio luminosity the optical output is much higher than in LBL objects (see Fig. 6), the optical flux is totally dominated by the non-thermal, featureless nuclear emission which makes any redshift estimation a very difficult task. Figure 3 (panel d) is an example of a featureless optical spectrum belonging to a source that could be a high luminosity HBL. Since there are 39 such

¹ IRAF is distributed by the National Optical Astronomy Observatories, which are operated by the Association of the Universities for Research in Astronomy, Inc., under cooperative agreement with the National Science Foundation

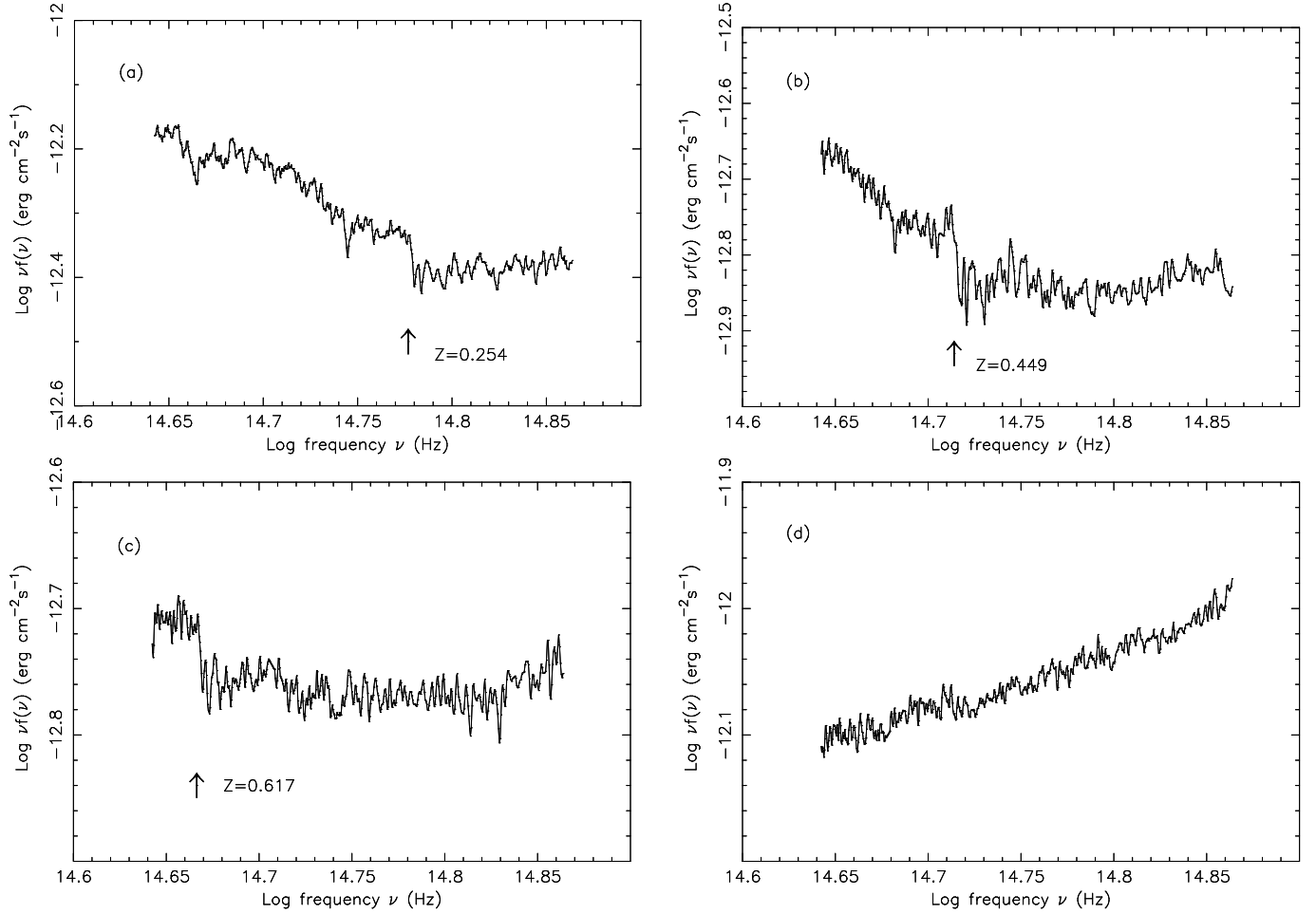


Fig. 3. SED of the optical region of the four BL Lac objects SHBLJ 104651.4–253545 (a), SHBLJ 044230.1–001830 (b), SHBLJ 020412.8–333342 (c) and SHBLJ 150340.6–154113 (d). Note that the optical output from the host galaxy (steep component) dominates the spectra of the sources (a), (b) and (c) at frequencies below the Ca H&K break (indicated by the arrow) while the nuclear non-thermal emission (flat component) is apparent at frequencies above the Ca H&K break. The optical spectrum of source (d) is instead totally dominated by its flat non-thermal component; no spectral features can be seen and therefore its redshift cannot be determined.

objects in the sample the fraction of high redshift ($z \gtrsim 0.8$) - high luminosity objects may be as high as $\sim 25\%$.

In principle these objects could also be very bright nearby radio sources; however if that were the case their radio flux distribution would be heavily biased towards high fluxes compared to that of the subsample of objects with a measured redshift. In Fig. 7 the distributions of 1.4 GHz radio fluxes for BL Lacs with measured redshift (solid line) and for the subsample of objects where the redshift could not be measured due to the featureless nature of the optical spectrum (dotted line) are shown. As can be seen, the latter objects strongly peak at low radio flux values indicating that they cannot be nearby very high luminosity objects that out-shine the host galaxy but rather high redshift high luminosity sources.

The only other alternative is that the luminosity of the host galaxies of these objects is extremely low contrary to the findings of Wurtz et al. (1997) and Urry et al. (2000).

We conclude that it is highly probable that the featureless objects are high redshift-high luminosity High Energy Peaked BL Lacs.

4.3. Rejected broad-lined candidates

The multi-frequency statistical selection criteria of the Sedentary survey have been estimated to be about 85% efficient. This paragraph deals with those candidates that although satisfied all the selection conditions of Paper I were at some point excluded from the sample because they were either reported in the literature as known emission line AGN or were not confirmed as BL Lacs by the optical identification process.

Specifically, in 8 cases the candidate HBLs have been found to be known emission line AGN and were rejected in Paper I; other 3 candidates have been identified as emission line AGN by Bauer et al. (2000) and Schwobe et al. (2000) after the publication of Paper I, while our optical spectroscopic campaign revealed 8 emission line AGN out of the 58 previously unclassified candidates that were observed.

All together the classification of all candidates in the Sedentary Survey revealed that only 19 out of the original 163 objects in the “HBL zone” showed emission lines that are too strong for a source to be called BL Lacertae object according

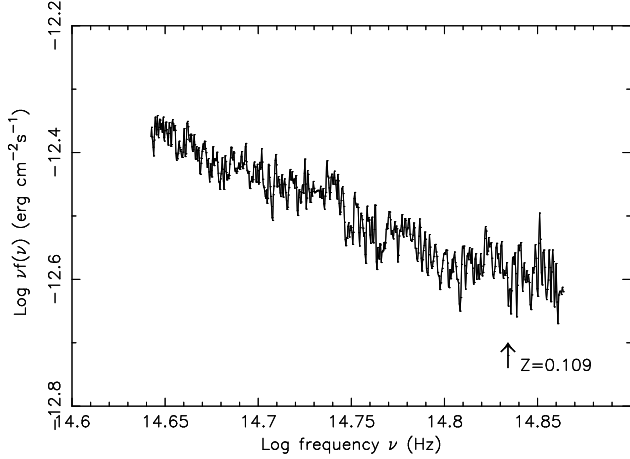


Fig. 4. SED of the optical region of SHBLJ 044127.4+150456. Most of the emission from this nearby ($z=0.109$) object is red i.e. steep and dominated by the optical output from the host galaxy. The nuclear non-thermal emission (flat component) is barely apparent at frequencies above the Ca H&K break (indicated by the arrow).

to the classification method of Marchã et al. (1996). The total level of contamination is therefore about 12%, well within the expected value of $\sim 15\%$ (see Paper I).

The 19 rejected emission line AGNs are listed in Table 3 where column 1 gives the RASS name, columns 2, 3 and 4 the fluxes in the X-ray (0.1–2.4 keV), radio (20 cm, from the NVSS survey) and the optical apparent V magnitude (from APM and COSMOS, see Paper I) respectively, column 5 the redshift, column 6 and 7 give the radio luminosity and the α_{ox} ; column 8 gives the reference for the optical identification.

These X-ray sources are mostly nearby, low radio luminosity emission line AGN with α_{ro} close to the selection threshold of 0.2. The radio emission of these sources is probably of non-nuclear origin and the X-ray emission may be unrelated to it.

From previous surveys we know that FSRQs with low $f_{\text{x}}/f_{\text{r}}$ are much more abundant than BL Lacs of similar $f_{\text{x}}/f_{\text{r}}$ both at high (e.g. in the 1Jy sample Stickel & Kühr (1993), Stickel et al. (1991)) and lower radio flux (e.g. 50 mJy, in the DXRBS survey Padovani et al. (1997), Landt et al. (2001)). Until recently X-ray strong (high $f_{\text{x}}/f_{\text{r}}$) FSRQ or HFSRQs (High energy peaked FSRQs) were instead thought to be very rare or altogether non-existent; however Padovani et al. (2003) discovered that a relative large number of HFSRQs indeed exist, although none with $f_{\text{x}}/f_{\text{r}}$ values as high as those required for inclusion in the sedentary survey.

If the relative abundance of FSRQ and BL Lacs were independent of $f_{\text{x}}/f_{\text{r}}$ (or, equivalently, on the position of the synchrotron peak energy) our survey, that includes 150 BL Lacs, should have detected several hundred extreme HFSRQs. Since we have possibly found only very few cases, all at relatively low redshifts and low radio power, we confirm with high statistical confidence that FSRQs very rarely (if at all) reach $f_{\text{x}}/f_{\text{r}}$ values so high as to satisfy condition 2) in our survey definition criteria ($f_{\text{x}}/f_{\text{r}} \geq 3 \times 10^{-10} \text{ erg cm}^{-2} \text{ s}^{-1} \text{ Jy}^{-1}$). In other

words the synchrotron component in broad lined Blazars do not reach peak energies as high as those found in HBL BL Lacs.

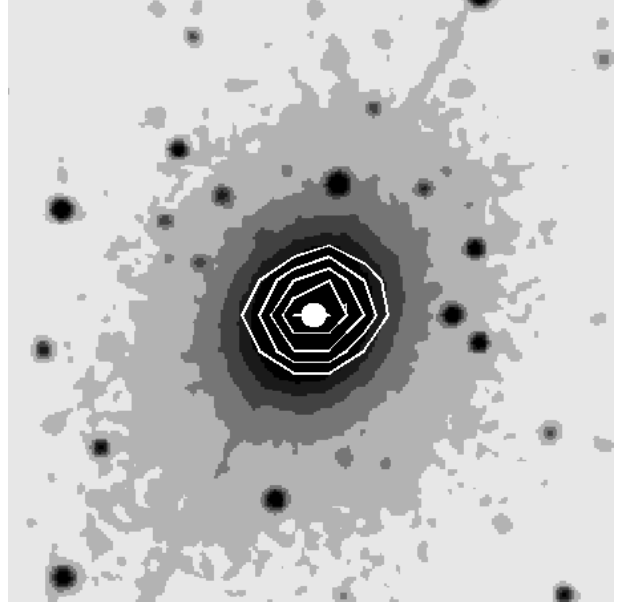


Fig. 5. The optical image and the radio iso-intensity contours of SHBL J020014.8+312545=NGC 0777, a nearby elliptical galaxy and candidate HBL in the survey. The NVSS position (filled symbol) of the flat spectrum radio source is consistent with that of nucleus of NGC 0777.

5. X-ray spectroscopy with *BeppoSAX*

The *BeppoSAX* X-ray Astronomy Satellite (see Boella et al. (1997) for a full description) was characterized by a very wide bandpass (0.1 \sim 200 keV) and therefore particularly well suited to study the X-ray spectrum of bright extragalactic objects like HBL BL Lacs. *BeppoSAX* successfully operated for a period of six years, from May 1996 to May 2002, during which it accumulated a large data archive, unique in terms of bandwidth, that can be used to determine the broad band X-ray spectrum of these sources.

A compilation of all the *BeppoSAX* spectral data for Blazars which were publicly available in March 2002 has been presented in Giommi et al. (2002a). In the following we update this work concentrating on the subset of objects belonging to the Sedentary survey and we complete the dataset by adding all the observations carried out after March 2002.

Twenty five objects of the Sedentary survey have been observed with *BeppoSAX* as part of different observing programs for a total of 50 pointings. Giommi et al. (2002a) considered several spectral models to fit the data and concluded that for HBL BL Lacs, which very often exhibit continuous convex curvature in the X-ray band, the model that best matches the data is a logarithmic parabola of the type

$$F(E) = K (E/E_*)^{-(a+b \cdot \text{Log}(E/E_*))} \quad (\text{ph/cm}^2/\text{s/keV}) \quad (1)$$

This model is particularly appealing since it can describe broad-band spectral curvature with only three free param-

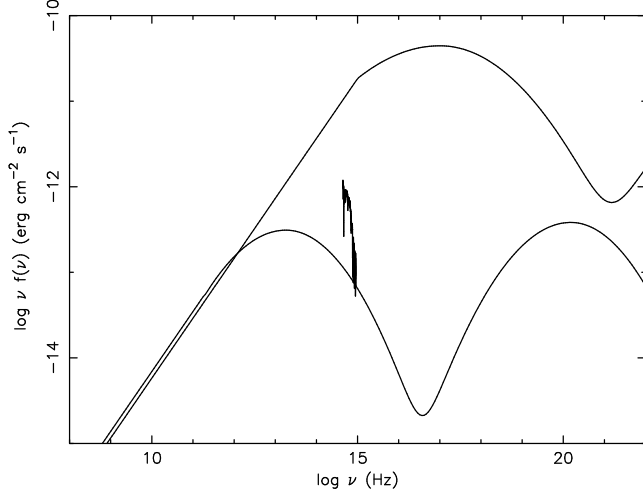


Fig. 6. Typical HBL and LBL spectral energy distributions compared to the SED of a typical giant elliptical galaxy. Note that the emission from the host galaxy is much more easily washed out by an HBL than by a LBL for the same radio flux.

ters K , a and b , just one more than a simple power law; in the following we assume $E_* = 1 \text{ keV}$. Massaro et al. (2004a) and Massaro et al. (2004b) carefully analyzed all the *BeppoSAX* observations of the bright HBL BL Lacs Mkn 421 and Mkn 501 and showed that the log-parabolic model is a good representation of the spectrum of these sources in all intensity states over the entire *BeppoSAX* energy bandpass. These authors also showed that the parameters of the logarithmic parabola model may provide information on the particle acceleration mechanism and can be used to easily calculate useful quantities such as an energy dependent photon index $\Gamma(E)$:

$$\Gamma(E) = a + 2b \text{Log}(E/E_*) \quad (2)$$

The parameter a is the photon index at the energy E_* , while b measures the curvature of the parabola. The peak frequency $\nu_p = E_p/h$, corresponding to the maximum in the $\nu - \nu F(\nu)$ plot, is given by:

$$E_p = E_* 10^{(2-a)/2b} \quad (\text{keV}) \quad (3)$$

and the maximum value is:

$$\nu_p F(\nu_p) = (1.60 \times 10^{-9}) K E_*^2 10^{(2-a)^2/4b} \text{ erg}/(\text{cm}^2 \text{ s}), \quad (4)$$

(Massaro et al. (2004a)).

The X-ray data analysis was carried out in a uniform way using the XANADU package (XIMAGE, XRONOS, XSPEC) and following the standard procedures described in the *BeppoSAX* documentation (<http://www.asdc.asi.it/bepposax/>). Spectral fitting was carried out with XSPEC (v. 11.0) using the calibration files available from the *BeppoSAX* Science Data Center. We have used data from the LECS and MECS experiments and, whenever the source was bright enough we also included the high energy PDS data. The results are reported in Table 4 where column 1 gives the source name, column 2 gives the date of the *BeppoSAX* observation, column 3 gives the instruments used for the analysis; columns 4, 5 and 6 give the best fit parameters (a , b and K) together with 1 sigma errors,

column 7 gives the reduced χ^2 , column 8 gives the 2–10 keV flux in units of $10^{-11} \text{ erg cm}^{-2} \text{ s}^{-1}$ and column 9 gives the peak energy derived using Eq. (3).

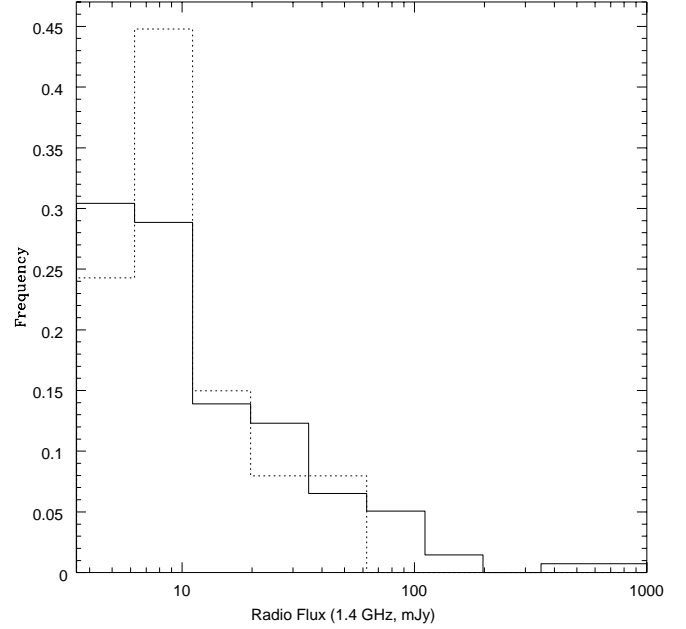


Fig. 7. The sky coverage corrected distributions of 1.4 GHz radio fluxes for BL Lacs with measured redshift (solid line) and for the subsample of objects where the redshift could not be measured due to the featureless nature of the optical spectrum (dotted line).

As can be seen, in all but a few cases (see notes below), the wide band X-ray spectra of the objects in the Sedentary Survey observed by *BeppoSAX* are satisfactorily described by the log-parabolic model. The curvature parameter (b) has been found to be positive, that is the spectrum is downward curved, in all sources with the exception of SHBL J020106.6+003401 and SHBLJ 123511.0-140322 (observation of July 1999) where the curvature estimation is very uncertain. The distribution of b is shown in Fig. 8 where it can be seen that the values of the curvature parameter measured with a reasonable accuracy cluster around values of $b \approx 0.4$ with a hint of a secondary peak at $b \approx 0.2$. This second peak, however is not statistically significant and larger samples would be needed to confirm or disprove it.

The energy where the emitted power is maximum (E_p) can be calculated from b and the measured photon index at 1 keV (a) using Eq. (3). In Fig. 9 the two quantities are plotted against each other. In this plot we have added the best fit values for Mkn 501 from Massaro et al. (2004b) to extend the E_p range to about 100 keV. The plotted quantities should be on a straight line if the curvature parameter were the same in all objects. From Fig. 9 we see that most of the sources actually lie along the $b = 0.4$ line in most intermediate cases ($0.1 < E_{\text{peak}} < 5 \text{ keV}$) but significant deviations are apparent both at very low

(PKS 2155-304) and at very high (Mkn 421 and Mkn 501 during flares) peak energies.

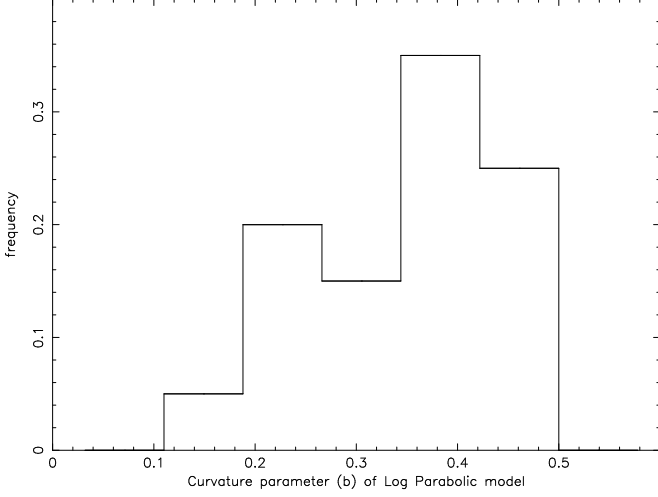


Fig. 8. The distributions of the curvature parameter (b) in the log parabolic model for the subsample of objects (18) for which the parameter b could be estimated with a statistical error less than 0.25

5.1. Notes on individual objects

5.1.1. SHBL J020106.3+003401

This is the only object in the sample which shows concave (upward instead of downward) curvature in the *BeppoSAX* X-ray spectrum. Most of this curvature is due to a feature above 6 keV where the statistics are not good enough to allow us to perform a detailed analysis. Moreover this source is within 3 arc-minutes from the QSO SDSS J020115.53+003135.1 which is clearly detected both in the *BeppoSAX* and in a Rosat PSPC image (although at a flux level lower than that of SHBL J020106.3+003401) that could contaminate the *BeppoSAX* data.

5.1.2. SHBL J074405.6+743358

The logarithmic parabola fit to the X-ray spectrum of this source is not a good representation of the data. The reduced χ^2 is 1.5 (17 d.o.f.) which is possibly due to the poor quality of the data and to a some flux excess above 4-5 keV.

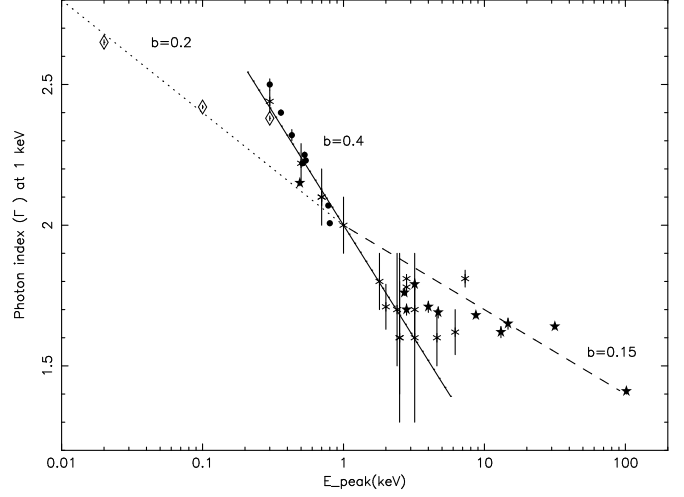


Fig. 9. The power law spectral index (Γ) at 1 keV (a) plotted against the peak energy. A strong correlation is present for E_p (as predicted by Eq. (3) if b is constant) values less than about 5 keV, above which Γ remains approximately constant. Crosses represent most of the objects listed in Table 3, diamonds are for PKS 2155-304, filled circles for Mkn 421 and filled stars for Mkn 501, which is not included in the sedentary survey because at the time of the RASS survey was in a very low state, but was added to this plot to extend the E_p dynamical range to about 100 keV. The solid, dotted and dashed lines represent the expected correlations for $b=0.4$, $b=0.2$ and $b=0.15$, respectively.

Table 4. Results of *BeppoSAX* spectral fittings

Source name SHBL J	Observation date	Instrument(s) used ^(*)	Best fit parameters			χ^2_r (d.o.f.)	flux ^(a)	E_p (keV)
(1)	(2)	(3)	a (4)	b (5)	K (6)	(7)	(8)	(9)
012308.7+342049	03-01-99	L M	1.9 ± 0.1	0.2 ± 0.1	$(6.7 \pm 0.6) 10^{-3}$	1.1(49)	1.70	1.8
	02-02-99	L M	1.8 ± 0.1	0.4 ± 0.1	$(6.0 \pm 0.7) 10^{-3}$	0.89(42)	1.30	1.8
013632.5+390559	09-01-01	L M	2.0 ± 0.1	0.5 ± 0.1	$(6.6 \pm 0.4) 10^{-3}$	1.11(44)	1.04	1.0
020106.3+003401	16-08-96	L M	2.5 ± 0.3	-0.2 ± 0.3	$(1.6 \pm 0.7) 10^{-3}$	1.25(20)	0.26	...
031951.9+184534	15-01-97	L M	1.6 ± 0.3	0.4 ± 0.2	$(2.3 \pm 0.7) 10^{-3}$	0.75(40)	0.7	3.2
032613.9+022515	20-01-98	L M	1.5 ± 0.3	0.7 ± 0.4	$(1.2 \pm 0.6) 10^{-3}$	0.95(20)	0.3	2.3
034923.2+115927	10-01-97	L M	1.7 ± 0.2	0.4 ± 0.2	$(2.4 \pm 0.6) 10^{-3}$	0.99(41)	0.6	2.4
041652.4+010524	21-09-96	M	2.3 ± 0.4	0.3 ± 0.3	$(6.4 \pm 1.8) 10^{-3}$	0.76(33)	0.84	0.3
050939.0+040036	11-02-99	L M	1.6 ± 0.2	0.5 ± 0.2	$(2.0 \pm 0.5) 10^{-3}$	0.90(35)	0.55	2.5
074405.6+743358	29-10-96	L M	2.5 ± 0.9	0.2 ± 0.7	$(1.3 \pm 1.3) 10^{-3}$	1.50(17)	0.14	0.1
093037.5+495025	25-11-98	L M	1.7 ± 0.1	0.3 ± 0.1	$(2.3 \pm 0.4) 10^{-3}$	1.04(42)	0.66	3.2
103118.6+505335	01-05-97	L M	2.1 ± 0.1	0.3 ± 0.1	$(6.2 \pm 0.3) 10^{-3}$	0.75(42)	1.02	0.7
110337.6+232931	04-01-97	L M P	1.6 ± 0.1	0.3 ± 0.1	$(11.7 \pm 0.8) 10^{-3}$	1.22(82)	3.72	4.6
	19-06-98	L M	1.9 ± 0.1	0.3 ± 0.1	$(11.7 \pm 0.6) 10^{-3}$	1.20(89)	2.51	1.5
110427.3+381231 ^(b)	29-04-97	L M	2.25 ± 0.01	0.45 ± 0.01	$(7.2 \pm 0.1) 10^{-2}$	1.31(132)	8.5	0.5
	30-04-97	L M	2.26 ± 0.01	0.47 ± 0.01	$(7.3 \pm 0.1) 10^{-2}$	0.75(136)	8.3	0.5
	01-05-97	L M	2.23 ± 0.01	0.43 ± 0.01	$(8.2 \pm 0.1) 10^{-2}$	1.06(132)	10.0	0.5
	02-05-97	L M	2.25 ± 0.01	0.43 ± 0.02	$(10.2 \pm 0.2) 10^{-2}$	0.86(127)	12.3	0.5
	03-05-97	L M	2.32 ± 0.02	0.44 ± 0.02	$(6.6 \pm 0.1) 10^{-2}$	0.97(100)	7.1	0.4
	04-05-97	L M	2.50 ± 0.02	0.48 ± 0.02	$(5.0 \pm 0.1) 10^{-2}$	1.16(100)	4.1	0.3
	05-05-97	L M	2.40 ± 0.01	0.45 ± 0.02	$(6.5 \pm 0.1) 10^{-2}$	1.11(100)	6.3	0.4
	21-04-98	L M P	2.07 ± 0.004	0.34 ± 0.006	$(18.8 \pm 0.1) 10^{-2}$	1.19(171)	31.0	0.8
	23-04-98	L M P	2.22 ± 0.004	0.37 ± 0.007	$(13.5 \pm 0.1) 10^{-2}$	1.02(169)	17.8	0.5
	22-06-98	L M P	2.07 ± 0.007	0.34 ± 0.008	$(14.4 \pm 0.1) 10^{-2}$	1.26(150)	23.9	0.8
	04-05-99	L M P	2.42 ± 0.004	0.42 ± 0.005	$(11.4 \pm 0.1) 10^{-2}$	1.11(141)	11.0	0.3
	26-04-00	L M P	1.81 ± 0.002	0.21 ± 0.002	$(22.7 \pm 0.1) 10^{-2}$	1.06(152)	62.5	2.8
111706.3+201407	09-05-00	L M P	1.88 ± 0.003	0.18 ± 0.003	$(19.4 \pm 0.1) 10^{-2}$	1.34(149)	49.5	2.2
	13-12-99	L M	2.44 ± 0.04	0.48 ± 0.05	$(6.7 \pm 0.3) 10^{-3}$	1.43(54)	0.61	0.3
112048.0+421212	01-05-97	L M	2.22 ± 0.07	0.4 ± 0.1	$(2.3 \pm 0.2) 10^{-3}$	0.40(25)	0.28	0.5
121158.6+224232	27-12-99	L M	1.8 ± 0.1	0.3 ± 0.1	$(0.9 \pm 0.2) 10^{-3}$	1.10(43)	0.24	2.2
	28-12-01	L M	1.62 ± 0.08	0.24 ± 0.07	$(2.1 \pm 0.2) 10^{-3}$	1.03(54)	0.75	6.2
	11-01-02	L M	1.4 ± 0.2	0.7 ± 0.2	$(1.7 \pm 0.3) 10^{-3}$	1.45(41)	0.52	2.7
122121.9+301037	12-07-99	L M	2.10 ± 0.03	0.37 ± 0.03	$(9.5 \pm 0.3) 10^{-3}$	0.78(88)	1.48	0.7
123511.0+140322	27-06-99	L M	1.4 ± 0.3	0.9 ± 0.4	$(0.8 \pm 0.2) 10^{-3}$	0.56(19)	0.19	2.2
	16-07-99	L M	2.6 ± 0.2	-0.4 ± 0.3	$(1.0 \pm 0.2) 10^{-3}$	0.46(19)	0.15	...
125731.9+241240	20-06-98	L M	1.6 ± 0.3	0.5 ± 0.3	$(3.8 \pm 1.2) 10^{-3}$	0.84(38)	1.11	2.5
141756.1+254356	13-07-00	L M	1.71 ± 0.08	0.47 ± 0.07	$(5.2 \pm 0.4) 10^{-3}$	1.15(49)	1.26	2.0
	23-07-00	L M	1.5 ± 0.2	0.7 ± 0.2	$(3.4 \pm 0.9) 10^{-3}$	0.84(36)	0.88	2.3
	27-07-00	L M	1.85 ± 0.08	0.30 ± 0.07	$(4.0 \pm 0.4) 10^{-3}$	1.25(49)	0.93	1.8
142832.6+424024	08-02-99	L M	1.81 ± 0.03	0.11 ± 0.03	$(6.6 \pm 0.3) 10^{-3}$	0.98(87)	2.03	7.3
151747.4+652523	05-03-97	L M	2.0 ± 0.2	0.4 ± 0.2	$(5.5 \pm 0.8) 10^{-3}$	1.30(39)	0.98	1.0
153500.9+532037	13-02-99	L M	2.0 ± 0.3	0.4 ± 0.3	$(1.4 \pm 0.5) 10^{-3}$	0.89(38)	0.25	1.0
215852.0+301331	20-11-96	L M P	2.42 ± 0.006	0.23 ± 0.01	$(49.3 \pm 0.4) 10^{-3}$	1.22(130)	5.59	0.1
	22-11-97	L M P	2.38 ± 0.008	0.36 ± 0.01	$(77.6 \pm 0.8) 10^{-3}$	1.28(108)	8.28	0.3
	04-11-99	L M	2.65 ± 0.009	0.20 ± 0.01	$(28.9 \pm 0.4) 10^{-3}$	1.16(103)	2.47	0.02
235907.9+303739	21-06-98	L M P	1.78 ± 0.03	0.25 ± 0.03	$(8.8 \pm 0.3) 10^{-3}$	1.35(91)	2.43	2.8

^(a) X-ray flux in the 2–10 keV band in units of 10^{-11} erg cm⁻²s⁻¹^(b) Spectral parameters taken from Massaro et al. (2004a)^(*) L=LECS; M=MECS; P=PDS

6. Broad-Band Spectral Energy Distributions and Synchrotron Peaks

One of the main motivations of the Sedentary Survey was the selection of a sizable *radio flux limited* sample of HBL BL Lacs, a type of sources that in the past have been discovered almost exclusively in X-ray surveys.

The very high X-ray to radio flux ratio that characterizes these objects is thought to be the result of synchrotron radiation extending to X-ray or even higher energies. To verify that this is indeed the case we have constructed the broad-band SED (in the usual $\text{Log}(\nu F(\nu))$ vs $\text{Log}(\nu)$ space) combining the *BeppoSAX* X-ray data (de-reddened using the cross sections of Morrison & McCammon (1983) setting the amount of absorbing material (N_H) equal to the Galactic value along the line of sight), with the (non-simultaneous) optical spectroscopy data from the sedentary identification campaign when available, and with non-simultaneous multi-frequency literature data taken from NED, from the NVSS 20 cm survey (Condon et al. (1998)), the Two Micron All Sky Survey (2MASS, Skrutskie et al. (1995)), the Sloan Digital Sky Survey (SDSS, Sloan Digital Sky Survey (2001)), the GSC2 catalog Lasker (1995); B.J. et al. (2000) and the Rosat All Sky Survey (Voges et al. (1999)).

6.1. 2MASS and GSC2 fluxes

The Two Micron All Sky Survey (2MASS) covers the full sky at near infra-red frequencies and allows us to add three flux measurements to our SEDs, at least for the brightest sources in our Survey. Indeed for all objects brighter that $V \sim 17.5$ a counterpart in the 2MASS Point Source Catalog (Cutri et al. (2003)) has been found.

We have converted J , H and K_s magnitudes from the 2MASS survey into monochromatic fluxes at 1.24, 1.66 and 2.16 microns assuming the following calibration (e.g. Cohen et al. (2003))

$$\begin{aligned} f(1.24\mu) &= 10^{-0.4(m_J - 15.51)} \text{ mJy} \\ f(1.66\mu) &= 10^{-0.4(m_H - 15.03)} \text{ mJy} \\ f(2.16\mu) &= 10^{-0.4(m_{K_s} - 14.56)} \text{ mJy} \end{aligned}$$

GSC2 F and J magnitudes have been converted as follows:

$$\begin{aligned} f(4.55 \cdot 10^{14} \text{ Hz}) &= 10^{-0.4(m_F - 16.16)} \text{ mJy} \\ f(6.00 \cdot 10^{14} \text{ Hz}) &= 10^{-0.4(m_J - 16.43)} \text{ mJy} \end{aligned}$$

all magnitudes have been de-reddened according to the prescriptions of Cardelli et al. (1989).

6.2. SED shapes

The SEDs of all objects for which *BeppoSAX* data are available are plotted in Figs. 10 through 34; for reasons of brevity the SED for the remaining objects, which include only a few points, are not plotted here but are available on-line at the following web site

<http://www.asdc.asi.it/sedentary/>

Although the data are not simultaneous, the $\nu f(\nu)$ dynamical range (\approx a factor of 1000) is much larger than the expected variability and allows us to characterize the broad band spectrum of HBL BL Lacs comparing the observed energy distribution to the expectations of a homogeneous Synchrotron Self-Compton (SSC) model adapted from Tavecchio, Maraschi & Ghisellini (1998). This model assumes that radiation is produced by a population of relativistic electrons emitting synchrotron radiation in a single zone of a jet that is moving at relativistic speed and at a small angle with respect to the line of sight. These photons are subsequently scattered by the same electrons to higher energies via the inverse Compton process (ignoring the Comptonization of external photons, which only affects the SED at γ -ray energies; e.g., Ghisellini et al. (1998)). The physical parameters that define the model are the jet radius, the Doppler factor, the magnetic field B , and four spectral parameters of the electron population, assumed to follow a power-law distribution which turns into a log parabolic distribution above a given energy: the normalization, the two spectral slopes, and the break energy. The Klein-Nishina cross section is used in the computation of the Compton scattering.

In a number of cases (e.g. SHBLJ012308.7+342049, SHBLJ041652.4+010524, SHBLJ103118.6+505335 etc.) the X-ray spectral data is consistent with being the smooth extrapolation of the same synchrotron emission observed at radio and optical frequencies, as predicted by a homogeneous single zone SSC model. In other cases (e.g. SHBLJ030195.1+184534, SHBLJ032613.9+022515, SHBLJ142832.6+424024 etc.), although the X-ray intensity is approximately located on the prediction of homogeneous SSC models, the low energy back-extrapolation of the *BeppoSAX* data clearly falls below the observed optical emission. This has been also noted in the detailed analysis of several *BeppoSAX* observations of Mkn 421 and Mkn 501 (Massaro et al. (2004a), Massaro et al. (2004b)) who interpreted this as due to the superposition of different emission components, the most energetic one possibly due to highly energetic electrons located in a very compact region inside the jet. Because of its small size the power output of this high energy component is only a fraction of the overall emission at optical frequencies but it becomes the dominant emission at very high energies where all other components have dropped well below their peak emission.

7. Discussion

We have presented the final, cleaned sample of the ‘‘Sedentary Survey of extreme HBL BL Lacs’’ which comprises 150 sources and is currently the deepest, largest, statistically complete and 100% identified flux-limited sample of BL Lacertae objects.

By means of multi-frequency literature data, our own optical spectroscopic observations and of wide band X-ray data from the *BeppoSAX* public archive we have investigated the local and the broad-band spectral properties of the sample.

We have found that:

1. The completion of the optical spectroscopy campaign, which led to the identification of all the objects in the survey (Paper III), fully confirmed the original assumption that a very high percentage of the sources in the initial sample were indeed BL Lac objects. In fact, 50 out of 58 previously unidentified candidates observed by us, or 86%, turned out to be BL Lacs, a similar percentage was found in the sources identified as part of different programs. This result validates the correctness of the selection method and the robustness of the preliminary results reported in Giommi et al. (1999) and Perri et al. (2002). The revised results on the statistical properties of the sample, including LogN-LogS, luminosity function and cosmological evolution, will be presented in a separate paper (Paper IV).

2. A significant fraction of the sources ($\sim 25\%$) displays a smooth non-thermal optical continuum without features due to either narrow emission lines or to the host galaxy. No redshift or luminosity can therefore be derived for these objects. However, since this condition only occurs when the nuclear non-thermal emission is much brighter than that of the host galaxy, a lower limit to the luminosity can be obtained setting the luminosity of the BL Lac equal to that of the host galaxy which is typically a giant elliptical with approximately constant absolute magnitude (e.g. Wurtz et al. (1997), Urry et al. (2000)). Unless these sources are all associated with (never observed) very low luminosity hosts they must be the most luminous objects in the survey. An independent indication that these sources are likely to be high redshift objects is provided by the progression of the dominance of the non-thermal over the galaxian component with redshift shown in Fig. 3 and by the distribution of radio fluxes shown in Fig. 7.

We conclude that the 25% of featureless sources in the sample are very likely intrinsically bright and therefore probably represent plentiful examples of the yet unreported *high radio luminosity-high energy peaked* BL Lacs. However, how luminous it remains to be determined. The existence of these sources would be at variance with the claimed inverse proportionality between radio power and synchrotron peak energy known as the “Blazar sequence”.

This luminosity sequence (Fossati et al. (1998)), which was interpreted as the direct consequence of differential cooling efficiencies in low and high radio power objects (Ghisellini et al. (1998)), was based on the absence of *low radio power - low ν_{peak}* and of *high radio power - high ν_{peak}* objects in a composite sample of BL Lacs and FSRQs detected in X-ray and radio flux limited surveys which, although each complete above its flux limit, probed widely different radio luminosity regimes.

The “Blazar sequence” has been recently tested using new deeper, larger and more homogeneous (i.e. with a single flux limit) samples of Blazars. The existence of low-radio luminosity-low ν_{peak} objects has been demonstrated by Padovani et al. (2003) and Caccianiga & Marchã (2004) who also showed that these are core-dominated radio sources just like the other BL Lacs and that their low radio power cannot be explained as the consequence of large orientation angles. In addition, the existence of high

radio luminosity-high ν_{peak} sources has been discussed by Giommi et al. (2002b) on the basis of preliminary results of the Sedentary Survey.

3. The relative abundance of FSRQ and BL Lacs of any f_x/f_r flux ratio is approximately of three-four FSRQ for each BL Lac (e.g. Stickel et al. (1991), Landt et al. (2001)). Although the selection criteria of the Sedentary Survey do not preclude the detection of FSRQs, we have found 150 extreme HBL BL Lacs and almost no FSRQs, instead of several hundred if the relative abundance of strongly lined and line-less Blazars were independent of f_x/f_r . Although a number of intermediate FSRQs have recently been found by Padovani et al. (2002), Padovani et al. (2003) it is clear that broad lined Blazars do not reach the very high synchrotron peak energies of HBL BL Lacs.
4. A few bright nearby elliptical galaxies have been found below the radio loud-radio quiet border ($\alpha_{ox} = 0.2$, see Table 2). These objects would normally be labelled “radio galaxies” or “normal ellipticals” and therefore removed from BL Lacs samples. However, these objects, which generally appear as point-like sources in the NVSS, may also be faint HBL BL Lacs whose non-thermal optical component is simply below the emission from the host galaxy. This situation must be expected towards the low end of the radio luminosity function.

In addition, strong flux variability, one of the defining properties of BL Lacs, and the position of the synchrotron peak (see Fig. 6), both have a strong influence on the ratio between the galactic and non-thermal optical flux, blurring the border between BL Lacs and radio galaxies. For example a borderline source that varied its non-thermal flux by a significant amount would be classified as a BL Lac when in a high state and as a radio galaxy when in the low state. Also, as shown in Fig. 6 two BL Lacs with identical radio flux but with synchrotron peaks at low and high energy (e.g. LBL and HBL) would also be classified differently depending on the position of the synchrotron peak.

5. Massaro et al. (2004a) and Massaro et al. (2004b) have shown that the wide band X-ray spectrum of the bright HBL BL Lacs like Mkn 421 and Mkn 501 can be satisfactorily described by a log-parabolic model in all intensity states (see Eq. (1)). We have then fit this model to the X-ray spectrum of all the objects in the survey that have been observed by *BeppoSAX* obtaining statistically acceptable fits in all but a few cases (see Table 4). The curvature parameter (b) has been found to be positive (i.e. the spectrum is downward curved) in almost all sources.
6. The broad band SEDs confirm that these objects are HBLs, that is their synchrotron emission extends to very high energies, sometimes well into the X-ray band. The X-ray data are generally located on the extrapolation for the radio and optical spectral distribution as predicted by homogeneous SSC models with the synchrotron power peaking at X-ray frequencies. However, the local strong X-ray curvature in a number of objects is not consistent with a simple back-extrapolation to optical frequencies suggesting that there may be more than one emission component.

7. The particularly energetic physical conditions that are necessary to produce the very high energy synchrotron photons observed imply that the corresponding Inverse Compton radiation must reach energies close to or within the TeV band. Indeed, even the source with the lowest synchrotron peak energy reported in Table 3 (i.e. PKS2155-304, $\nu_{peak} = 0.02-0.3$ keV) has been detected at TeV frequencies (Chadwick et al. (1999), Hinton (2003)). It is therefore natural to expect that many of the sources in the Sedentary survey are TeV emitters and that the brightest and closest ones may be detectable by the present generation of Cherenkov telescopes, especially during flares. However, despite this obvious prediction only 3 (Mkn421=SHBL J110427.3+381231, PKS2155-304=SHBL J215852.0-301331 and H1426+428=SHBL J142832.6+424024) of the 6 presently established TeV BL Lacs are actually included in our survey. Mkn 501, 1ES2344+514 and 1ES1959+650, the remaining TeV Blazars, all displayed synchrotron peak energies well into the hard X-ray band (Massaro et al. (2004b), Giommi et al. (2000), Krawczynski et al. (2004)) during strong outbursts but never reached (not even during the strongest flare) a soft X-ray flux ratio high enough to meet the f_x/f_r condition necessary to be part of the Sedentary survey. Most of the X-ray variations in these sources were in fact confined to the hard X-ray band, close to the maximum of their synchrotron power and above the Rosat bandpass. This implies that synchrotron peak energies in the hard X-ray band are not necessarily located on the smooth extrapolation of the lower energies spectrum, but may be due to additional, very energetic emission components that only emerge above the Rosat X-ray band. The existence of such sub-components is consistent with the observed difference between the shape of the overall SED and the local X-ray spectral curvature in many objects (see Figs. 13, 14, 17, 22, 28, 30 and 31). It is likely that TeV emission is associated with these components, some of which may not always be detectable at soft X-ray frequencies because they could be outshone by the main or by some other less energetic synchrotron component. This would be consistent with the existence of the recently reported “X-ray orphan” TeV flares (Krawczynski et al. (2004)), that is TeV flare emission not correlated to soft X-ray flares and that this lack of correlation should be expected in other objects. Simultaneous sensitive hard-X-ray observations are obviously desirable and could be achieved in the short term by organizing TeV observations with the Swift spacecraft and on the medium term with the next generation of hard X-ray imaging telescopes.

Acknowledgements. This work is partly based on *BeppoSAX* X-ray data taken from the *BeppoSAX* public archive hosted at the ASI Science Data Center (ASDC), Frascati, Italy, and on

Optical spectroscopy observations performed at the European Southern Observatory, La Silla, Chile, (Proposals ESO n. 67.B-0222(A), 71.B-0582(A) and 71.B-0582(B)), Telescopio Nazionale Galileo, La Palma, Canarian Islands (proposals AOT5/02A, AOT6/02B, AOT7/03A) and Kitt Peak National Observatory.

This research has also made use of data taken from the following on-line services

- the NASA/IPAC Extragalactic Database (NED)
- the ESO on-line Digitized Sky Survey
- the Two Micron All Sky Survey, a joint project of the University of Massachusetts and IPAC, funded by NASA and NSF
- the Sloan Digital Sky Survey archive, which is funded by the Alfred P. Sloan Foundation
- the Guide Star Catalog-II, which is a joint project of the Space Telescope Science Institute and the Osservatorio Astronomico di Torino.

The authors are grateful to E. Massaro for useful suggestions.

References

- Anderson, S. F., Voges, W., Margon, B., et al. 2003, *AJ*, 126, 2209
- Bade, N., Beckmann, V., Douglas, N. G., et al. 1998a, *A&A*, 334, 459
- Bade, N., Engels, D., Voges, W., et al. 1998b, *A&AS*, 127, 145
- Bade, N., Fink, N., & Engel, D. 1994, *A&A*, 286, 381
- Bauer, F., Condon, J., Thuan, T., & Broderick, J. 2000, *ApJS*, 129, 547
- Beckmann, V. 2000, PhD thesis, Hamburg University, <http://www.sub.uni-hamburg.de/disse/330/vbdiss.html>
- Beckmann, V., Bade, N., & Wucknitz, O. 1999, *A&A*, 352, 395
- Beckmann, V., Engels, D., Bade, N., & Wucknitz, O. 2003, *A&A*, 401, 927
- B.J., M., Greene, G. R., Lattanzi, M. G., & Pirenne, B. 2000, in *ASP Conf. Ser., ADASS IX*, ed. V. C. . C. D. Manset N., Vol. 216, 145–148
- Boella, G., Chiappetti, L., Conti, G., et al. 1997, *A&AS*, 122, 327
- Bohringer, H., Voges, W., Huchra, J., et al. 2000, *ApJS*, 129, 435
- Buchalter, A., Helfand, D., Becker, R., & White, R. 1998, *ApJ*, 494, 503
- Caccianiga, A. & Marchã, M. J. 2004, *MNRAS*, 348, 937
- Cao, L., Wey, J.-Y., & Hu, J.-Y. 1999, *A&AS*, 135, 243
- Cardelli, J. A., Clayton, G. C., & Mathis, J. S. 1989, *ApJ*, 345, 245
- Chadwick, P., Lyons, K., McComb, T., et al. 1999, *ApJ*, 513, 161
- Cohen, M., Wheaton, W. A., & Megeath, S. T. 2003, *AJ*, 126, 1080
- Condon, J. J., Cotton, W. D., Greisen, E. W., et al. 1998, *AJ*, 115, 1693
- Cutri, R., Skrutskie, M., & van Dyk, S., e. a. 2003, Univ. of Massachusetts and IPAC on-line catalog.
- De Vaucouleurs, G., De Vaucouleurs, A., H.G., C. J., et al. 1991, Third Reference Catalogue Of Bright Galaxies, Version 3.9
- Falomo, R., Pesce, J., & Treves, A. 1993, *ApJ*, 411, 63
- Fisher, J., Hasinger, G., Schwöpe, A., et al. 1998, *Astron. Nachr*, 319, 347
- Fossati, G., Maraschi, L., Celotti, A., Comastri, A., & Ghisellini, G. 1998, *MNRAS*, 299, 433
- Ghisellini, G., Celotti, A., Fossati, G., Maraschi, L., & Comastri, A. 1998, *MNRAS*, 301, 451

- Giommi, P., Capalbi, M., Fiocchi, M., et al. 2002a, in *Blazars Astrophysics with BeppoSAX and Other Observatories*, ed. P. Giommi, E. Massaro, & G. Palumbo, 63
- Giommi, P., Menna, M. T., & Padovani, P. 1999, *MNRAS*, 310, 465
- Giommi, P., Padovani, P., & E., P. 2000, *MNRAS*, 317, 743
- Giommi, P., Padovani, P., Perri, M., Landt, H., & Perlman, E. 2002b, in *Blazars Astrophysics with BeppoSAX and Other Observatories*, ed. P. Giommi, E. Massaro, & G. Palumbo, 133
- Giommi, P., Perri, M., Piranomonte, S., & Padovani, P. 2002c, in *Blazars Astrophysics with BeppoSAX and Other Observatories*, ed. P. Giommi, E. Massaro, & G. Palumbo, 123
- Giommi, P., Piranomonte, S., Perri, M., & Padovani, P. 2004, in preparation
- Hewett, P., Foltz, C., & Chaffee, F. 1995, *AJ*, 109, 1498
- Hinton, J. 2003, for the H.E.S.S. Collaboration, 2nd VERITAS Symposium, Chicago
- Irwin, M., Maddox, S., & McMahon, R. G. 1994, *Spectrum*, 2, 14
- Krawczynski, H., Hughes, B., Horan, D., et al. 2004, *ApJ*, 601, 151
- Landt, H., Padovani, P., & Giommi, P. 2002, *MNRAS*, 336, 945
- Landt, H., Padovani, P., Perlman, E. S., et al. 2001, *MNRAS*, 323, 757
- Lasker, B. M., e. a. 1995, in in ESA SP-379, *Future Possibilities for Astrometry in Space*, ed. v. L. F. . G. T.-D. Perryman M.A.C., 137
- Marchã, M. J. M., Browne, I. W. A., Impey, C. D., & Smith, P. S. 1996, *MNRAS*, 281, 425
- Massaro, E., Perri, M., Giommi, P., & Nesci, R. 2004a, *A&A*, 413, 489
- Massaro, E., Perri, M., Giommi, P., Nesci, R., & Verrecchia, F. 2004b, *A&A*, 422, 103
- Morrison, R. & McCammon, D. 1983, *ApJ*, 270, 119
- NED Redshift, T. 1992, The NED Team Redshift obtained from literature by the NED TEAM prior to November 1992
- Padovani, P., Costamante, L., Ghisellini, G., Giommi, P., & Perlman, E. 2002, *ApJ*, 581, 895
- Padovani, P. & Giommi, P. 1995, *MNRAS*, 277, 1477
- Padovani, P., Giommi, P., & Fiore, F. 1997, *MmSAI*, 68, 147
- Padovani, P., Perlman, E., Landt, H., Giommi, P., & Perri, M. 2003, *ApJ*, 588, 128
- Perri, M., Giommi, P., , Piranomonte, S., & Padovani, P. 2002, in *Blazars Astrophysics with BeppoSAX and Other Observatories*, ed. P. Giommi, E. Massaro, & G. Palumbo, 119
- Piranomonte, S., Perri, M., Giommi, P., Padovani, P., & Landt, H. 2004, submitted to *A&A*
- Polonsky, E., Vennes, S., Thorstensen, J., Mathioudakis, M., & Falco, E. 1997, *ApJ*, 486, 179
- Puchnarewicz, E., Mason, K., Cordova, F., et al. 1992, *MNRAS*, 256, 589
- Rector, T. A., Stocke, J. T., Perlman, E. S., Morris, S. L., & Gioia, I. M. 2000, *AJ*, 120, 1626
- Reimers, D., Koehler, T., & Wisotzki, L. 1996, *A&AS*, 115, 235
- Schachter, J., Stocke, J., Perlman, E., et al. 1993, *ApJ*, 412, 541
- Schneider, D. P., Schmidt, M., & Gunn, J. 1994, *AJ*, 107, 1245
- Schwope, A., Hasinger, G., Lehmann, I., et al. 2000, *Astron. Nachr.*, 321, 1
- Skrutskie, M. F., Beichman, C., Capps, R., et al. 1995, *Bulletin of the American Astronomical Society*, 27, 1392
- Sloan Digital Sky Survey, T. 2001, Early release as obtained in June 5, 2001, Sloan Digital Sky Survey 2001
- Stickel, M., Fried, J. W., Kühr, H., Padovani, P., & Urry, C. M. 1991, *ApJ*, 374, 431
- Stickel, M. & Kühr, H. 1993, *A&AS*, 101, 521
- Urry, C. M. & Padovani, P. 1995, *PASP*, 107, 803
- Urry, C. M., Scarpa, R., O'Dowd, M., et al. 2000, *ApJ*, 532, 816
- Voges, W., Aschenbach, B., Boller, T., et al. 1999, *A&A*, 349, 389
- White, R. L., Becker, R. H., Gregg, M., et al. 2000, *ApJS*, 126, 133
- Wurtz, R., Stocke, J. T., Ellingson, E., & Yee, H. K. C. 1997, *ApJ*, 480, 547
- Yentis, D., Cruddace, R., & Gursky, H. 1992, in *Digitised Optical Sky Surveys*, ed. H. MacGillivray & E. Thomson (Dordrecht: Kluwer Academic Publishers), 67

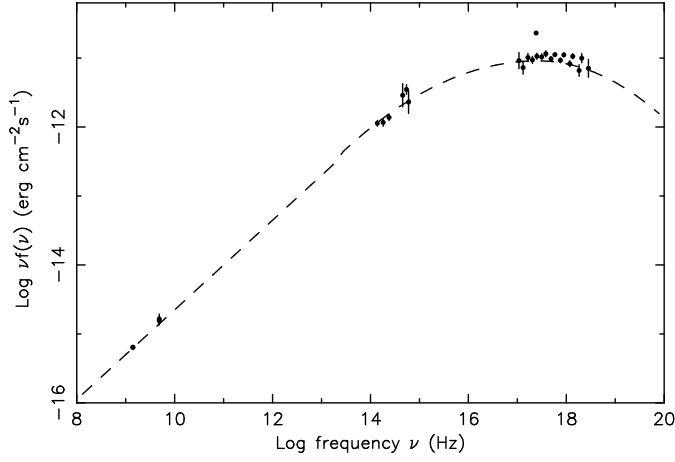


Fig. 10. Spectral Energy Distribution of SHBL J012308.7+342049

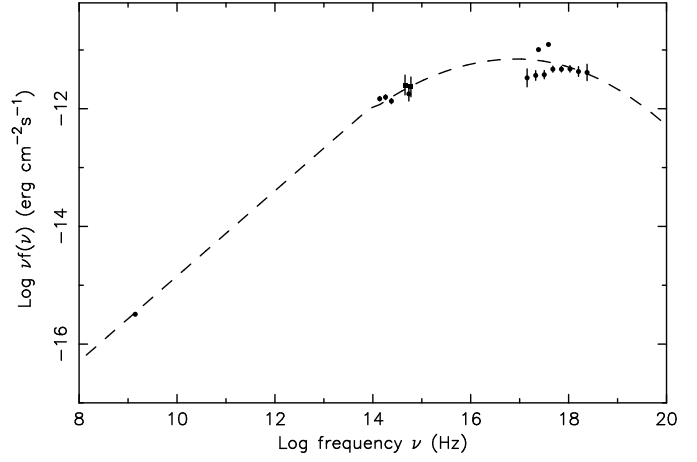


Fig. 13. Spectral Energy Distribution of SHBL J031951.9+184534

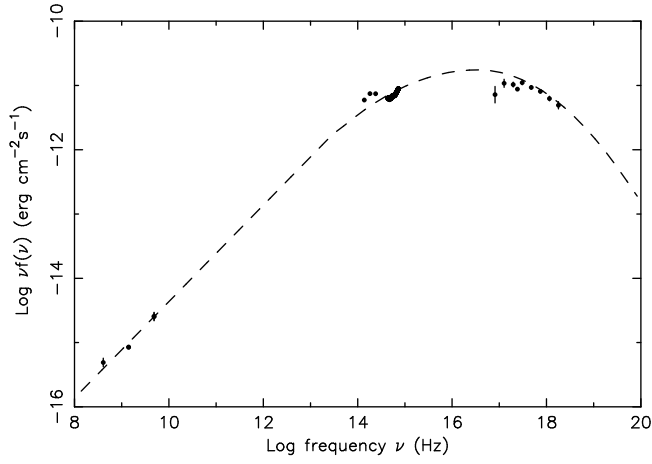


Fig. 11. Spectral Energy Distribution of SHBL J013632.5+390559

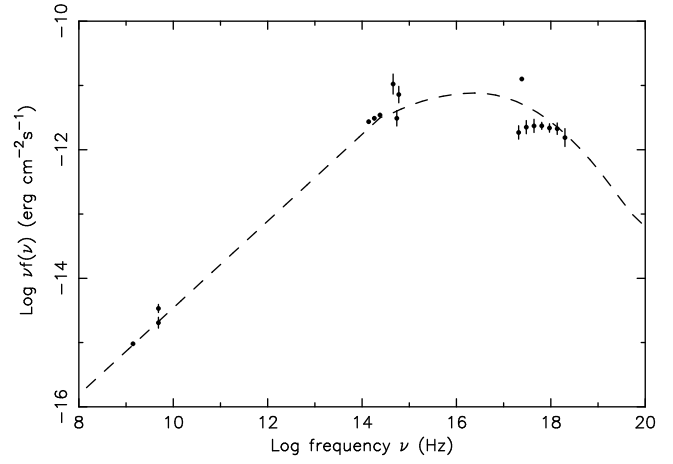


Fig. 14. Spectral Energy Distribution of SHBL J032613.9+022515

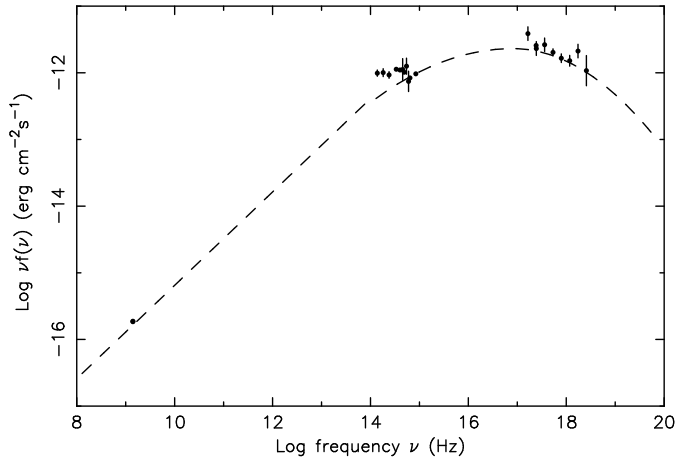


Fig. 12. Spectral Energy Distribution of SHBL J020106.3+003401

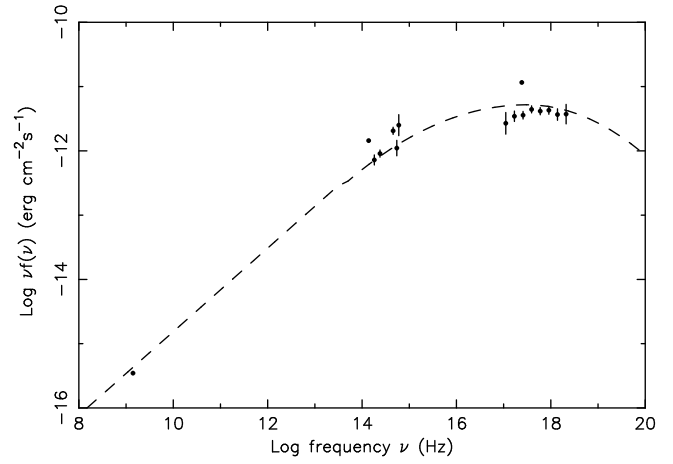


Fig. 15. Spectral Energy Distribution of SHBL J034923.2-115927

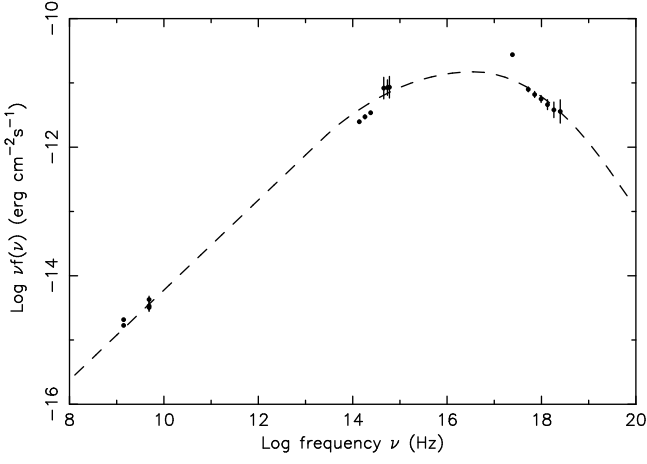


Fig. 16. Spectral Energy Distribution of SHBL J041652.4+010524

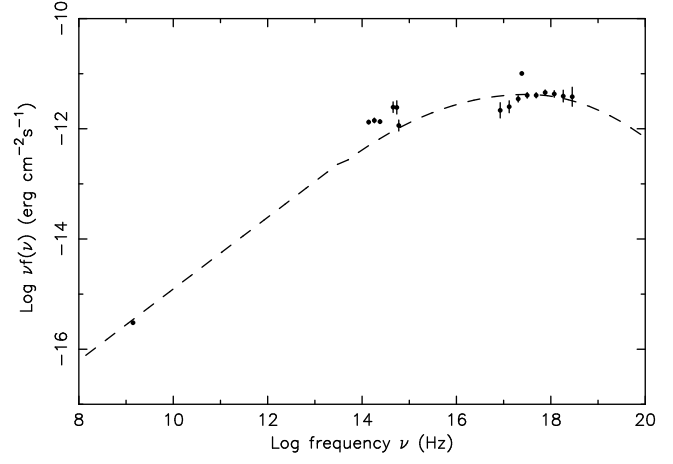


Fig. 19. Spectral Energy Distribution of SHBL J093037.5+495025

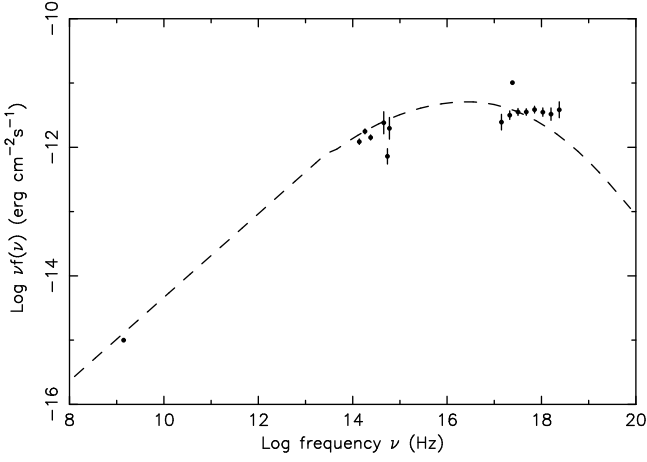


Fig. 17. Spectral Energy Distribution of SHBL J050939.0-040036

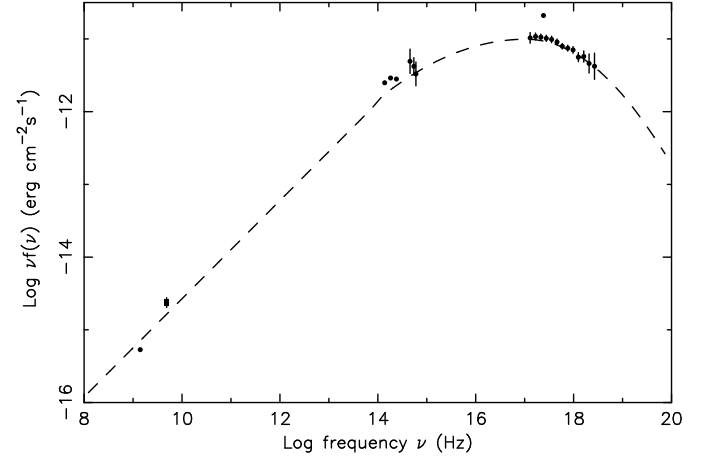


Fig. 20. Spectral Energy Distribution of SHBL J103118.6+505335

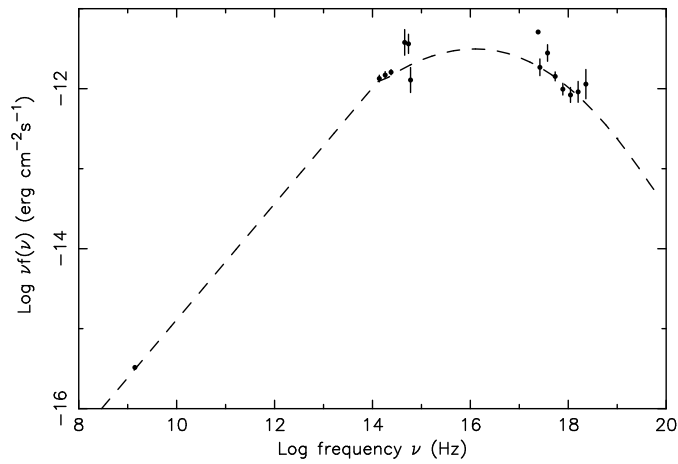


Fig. 18. Spectral Energy Distribution of SHBL J074405.6+743358

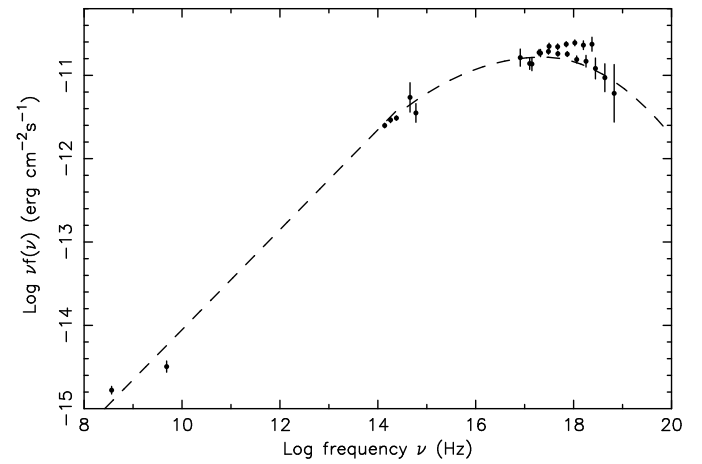


Fig. 21. Spectral Energy Distribution of SHBL J110337.6-232931

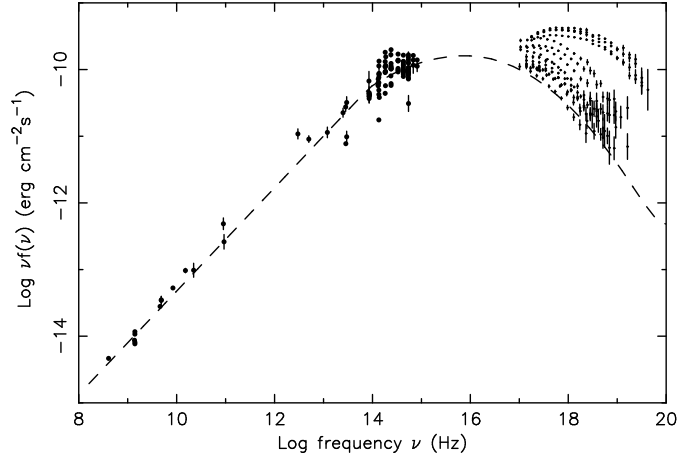


Fig. 22. Spectral Energy Distribution of SHBLJ 110427.3+381231=MKN 421

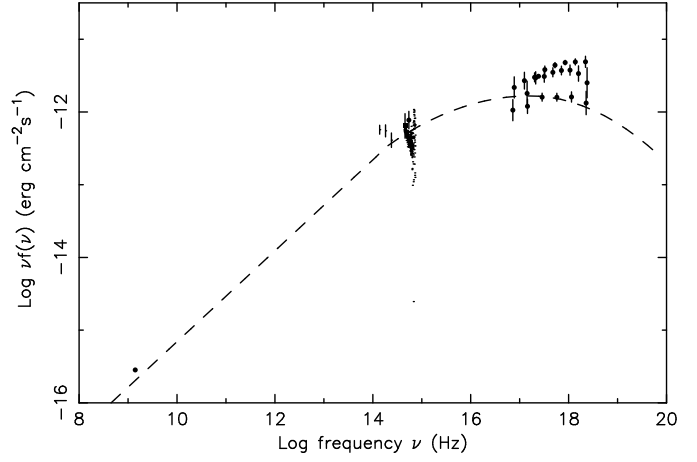


Fig. 25. Spectral Energy Distribution of SHBLJ 121158.6+224232

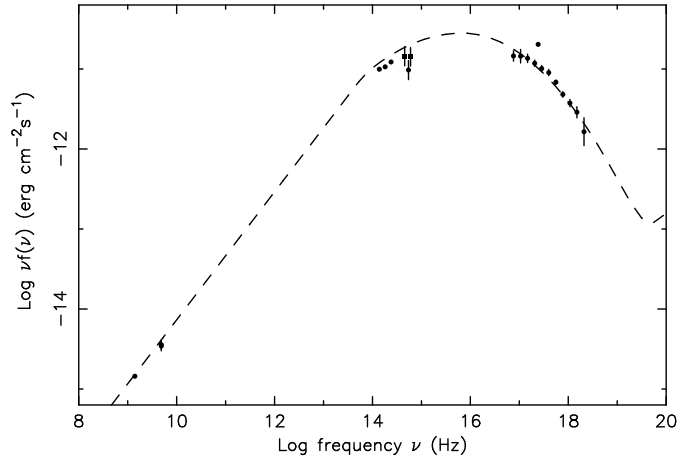


Fig. 23. Spectral Energy Distribution of SHBLJ 111706.3+201407

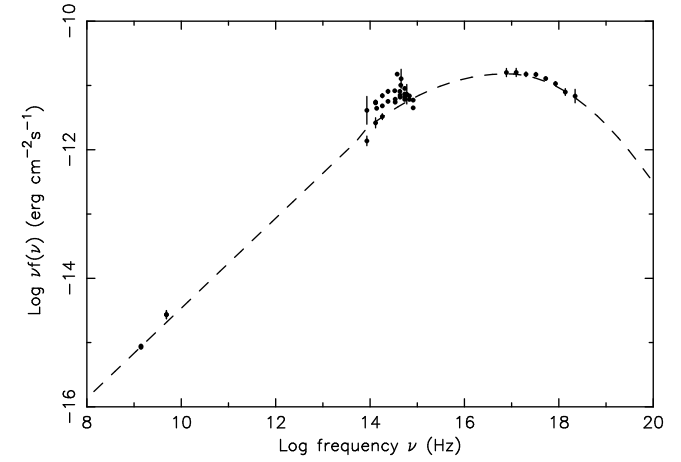


Fig. 26. Spectral Energy Distribution of SHBLJ 122121.9+301037

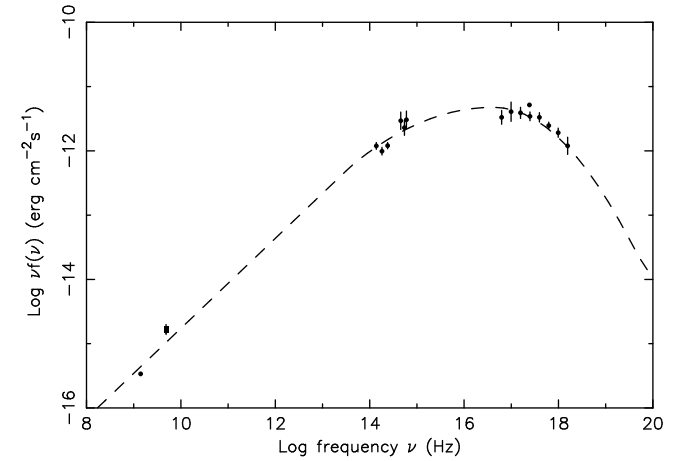


Fig. 24. Spectral Energy Distribution of SHBLJ 112048.0+421212

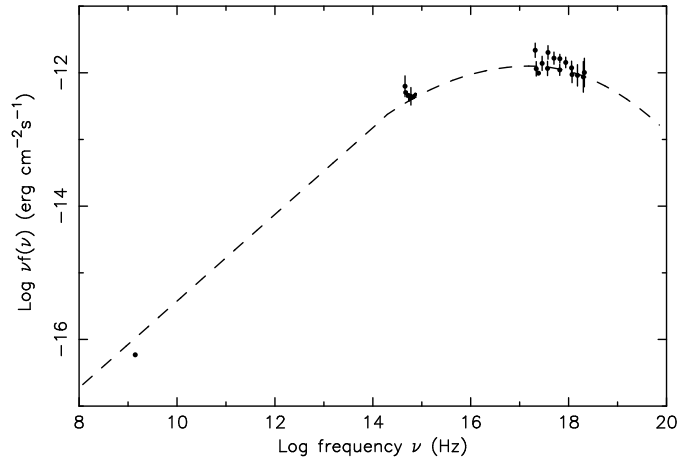


Fig. 27. Spectral Energy Distribution of SHBLJ 123511.0-140322

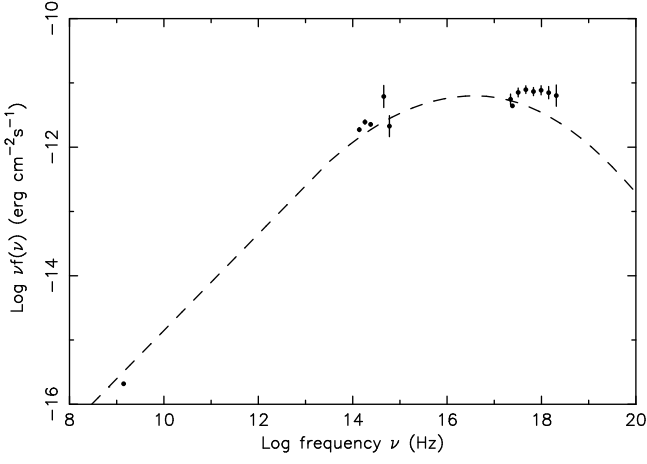


Fig. 28. Spectral Energy Distribution of SHBLJ 125731.9+241240

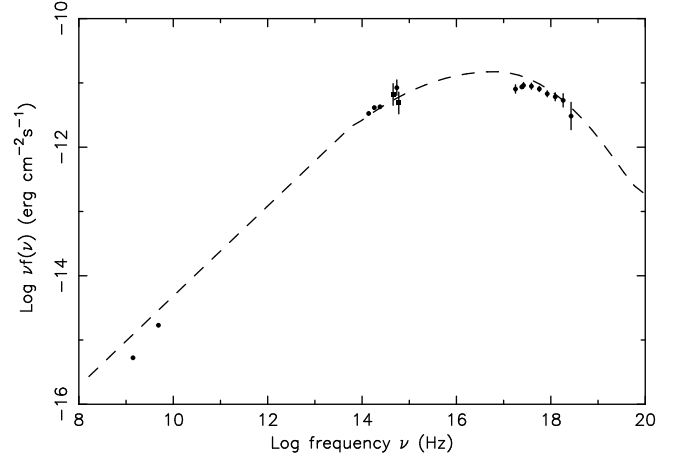


Fig. 31. Spectral Energy Distribution of SHBLJ 151747.4+652523

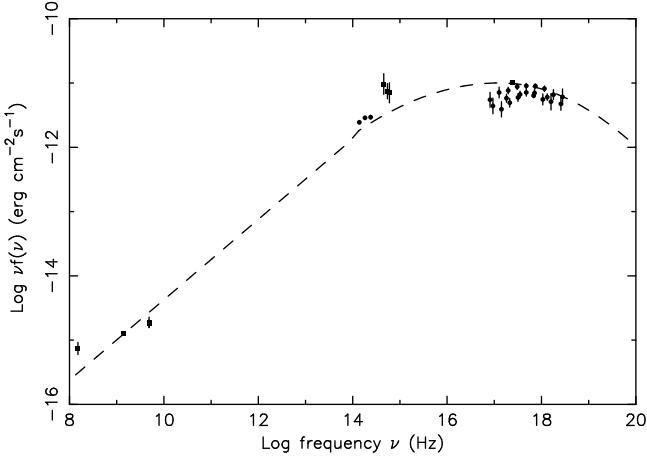


Fig. 29. Spectral Energy Distribution of SHBLJ 141756.1+254356

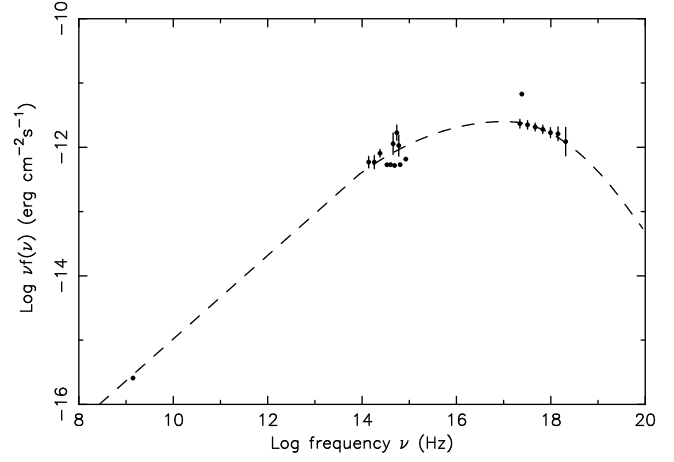


Fig. 32. Spectral Energy Distribution of SHBLJ 153500.9+532037

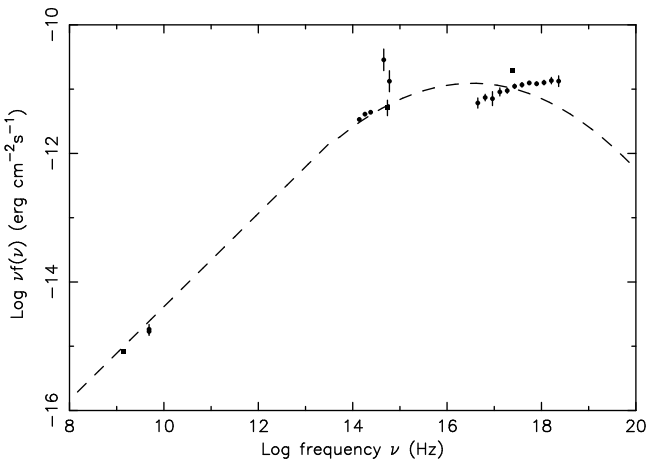


Fig. 30. Spectral Energy Distribution of SHBLJ 142832.6+424024

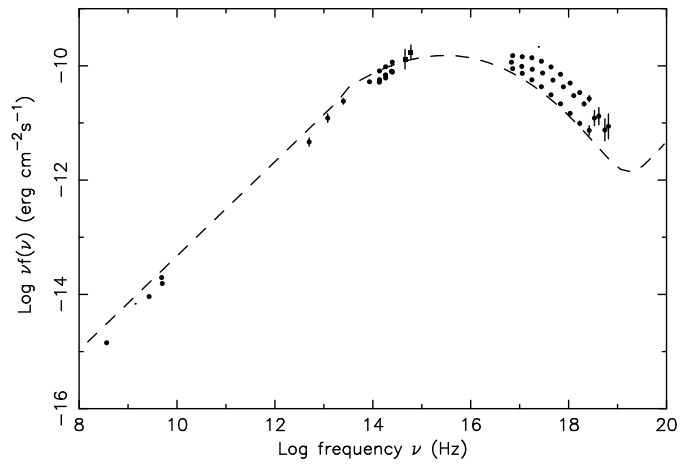


Fig. 33. Spectral Energy Distribution of SHBLJ 215852.0-301331=PKS 2155-304

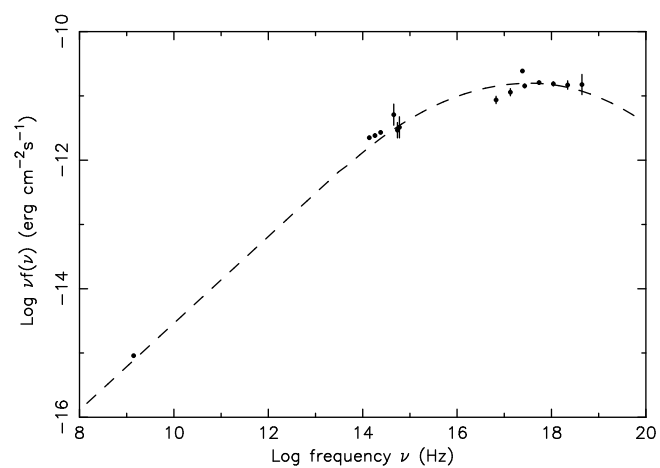


Fig. 34. Spectral Energy Distribution of SHBLJ 235907.9-303739